PREDICTING TENDERNESS OF BEEF USING

MACHINE VISION

By

ANAND LAKSHMIKANTH

Bachelor of Engineering

College of Agricultural Engineering

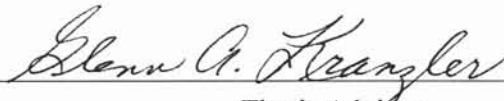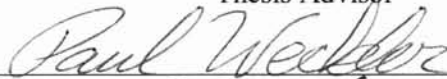Tamil Nadu Agricultural University

Kumulur, Tamilnadu, India

1998

Submitted to the Faculty of the
Graduate College of the
Oklahoma State University
in partial fulfillment of
the requirements for
the Degree of
MASTER OF SCIENCE
December, 2002

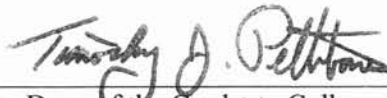PREDICTING TENDERNESS OF BEEF USING

MACHINE VISION

Thesis Approved:

Glenn A. Kranzler
Thesis Advisor

Paul Weckler

_Wm. _____

Timothy J. Pethtonz
Dean of the Graduate College

ACKNOWLEDGMENTS

TABLE OF CONTENTS

LIST OF TABLES

LIST OF FIGURES

NOMENCLATURE

AMSA	American Meat Science Association
ANN	Artificial Neural Network
AT	Armour Tenderometer
BPNN	Backpropagation Neural Network
CIE	Commission Internationale de l'Eclairage
CWT	Continuous Wavelet Transform
DWT	Discrete Wavelet Transform
FAPC	Food and Agricultural Products Center
FT	Fourier Transform
GLDH	Gray-Level Difference Histogram
GLCM	Gray-Level Cooccurence Matrix
HSI	Hue-Saturation-Intensity
MIRINZ	Meat Industry Research Institute of New Zealand
MRA	Multiresolution Analysis
MLR	Multi-Linear Regression
MSE	Mean Square Error
NBIAP	National Beef Instrument Assessment Plan
NCBA	National Cattlemen's Beef Association
NIR	Near-Infrared

PCA   Principal Component Analysis

PLS   Partial Least Squares

RGB   Red-Green-Blue

STFT   Short-Time Fourier Transform

USDA   United States Department of Agriculture

UV   Ultraviolet

VIA   Video Image Analysis

WT   Wavelet Transform

WBS   Warner-Bratzler Shear-force

ABSTRACT

Tenderness is a critical factor in consumer perception of beef quality. A computer vision system was developed to predict 14-day aged cooked-beef tenderness. Steak samples (n=186) were acquired from regional packing plants and imaged at 1-day postmortem. Steak images were decomposed using Haar and Daubechies wavelets. Textural features were derived from wavelet transforms (WT). Gray-level difference histograms (GLDH) were extracted from the decomposed images.

WT- and GLDH-based features from the red-green-blue (RGB) and the CIE L* a* b* color spaces were combined, separately. Features were reduced in number by linear regression to eliminate redundancy. The two separate reduced sets of features were pre-processed using principal component analysis. Each set of features was split into training and test sets with a count ratio of 3:1. Statistical and neural network analysis was performed to predict 14-day postmortem Warner-Bratzler shear-force (WBS) tenderness scores. Stepwise regression yielded a correlation coefficient of 0.57 for WT-based features and 0.48 for GLDH-based features. A backpropagation (BPNN) neural network model with Bayesian regularization was developed. The BPNN network predicted WBS scores with a correlation coefficient range of 0.57-0.59 for WT-based features (training and test sets) and 0.55 and 0.31 for training and test sets, respectively, for GLDH-based features.

A t-test analysis was performed to determine the ability of the model to sort "certified tender" samples from "not certified tender" samples, at certification levels of 10% to 100%, for both training and test data sets. This approach was more applicable because of an insufficient number of "tough" samples in the data. Except for the 10% and 70% certification levels in the test set of GLDH-based features, there was a significant difference ($\alpha=0.05$) between the "certified tender" and "not certified tender" categories. For both WT- and GLDH-based features, 71.4% and 66.7% of "tough" samples in the test and training set, respectively, were successfully sorted from the "tender" samples.

WT-based features were found to be more effective than GLDH-based features in predicting 14-day postmortem WBS tenderness scores, and in terms of accurately sorting "tender" and "tough" samples. The system was capable of sorting and categorizing fresh beef samples on the basis of aged-beef tenderness with moderate accuracy.

CHAPTER I

INTRODUCTION

<u>Background</u>

Oklahoma ranks fifth in the nation in receipts from cattle production. The output represents 65% of the total state agricultural receipts, provides jobs for 105,000 laborers, and accounts for approximately $2.4 billion of the Gross State Product (OBIC, 2002). The motto of the National Cattlemen's Beef Association (NCBA) is "… to maximize consumer confidence in and acceptance of beef by focusing the industry's attention on beef quality assurance through the use of science, research, and educational initiatives" (NCBA, 2002). Beef quality is what accounts for profits for beef producers, and visual grading by USDA-approved graders assigns the quality. The manual grading procedure involves a visual examination of the characteristics of the *Longissimus dorsi* muscle, commonly known as the ribeye. The carcass is sectioned between the 12th and the 13th rib to expose the ribeye. This method of visual grading has often been criticized for being too subjective and error-prone. In a beef packing plant, a carcass passes by every 9-18 s, giving the grader a limited amount of time to determine grade. In addition, emotional strain caused by monotonous work, inadequate lighting, and dangerous working conditions make it difficult for manual graders to maintain accuracy.

Instrumented carcass evaluation provides an objective system of grading that ensures consistency and enables value-based marketing. The National Beef Instrument Assessment Plan of the National Livestock and Meat Board (Schutte et al., 1998) suggested the application of instrumented grading for objective carcass evaluation. The Plan stated that the system of grading should be accurate, tamper proof, capable of "on-line" operation, and provide repeatable results. Video image analysis (VIA) was identified as the most promising technique for objective grading, and was thus been given top research priority. This technology has been an active topic of research, because it simulates the human eye for grade assessment. Kranzler et al. (1998) developed a VIA system to measure ribeye area, marbling or intramuscular fat, lean color, and to assign a quality grade based on USDA standards. Results from the VIA system were compared with those of expert graders and found to be statistically equivalent. Jeyamkondan et al. (2000) utilized the VIA system developed at Oklahoma State University to segment the ribeye from beef steak images and predict quality grade. The quality grades predicted by the VIA system were statistically equivalent to the grades assigned by expert graders for the same samples. The R^2 value for prediction was 0.72. These tests indicated that the VIA system was highly suitable for objective, on-line grading.

Beef Tenderness

Tenderness is a critical factor in consumer perception of beef quality (Koohmaraie et al., 2002). The 1994 National Beef Quality Audit (Smith et al., 1995) and various consumer surveys indicate 25% of beef eating experiences are unsatisfactory.

Consumers have ranked beef tenderness as the most important characteristic for palatability, along with juiciness and flavor.

Current USDA beef grading standards do not account for tenderness. These standards assign two grades; yield and quality (Biju, 1998). Graders assess the ribeye area, rib fat thickness, and carcass weight to determine yield grade. Ribeye marbling, color features, and maturity are judged to assign quality grade. Unfortunately, tenderness is a quality that is not easily discernable to the human eye. An accepted measure of tenderness is the Warner-Bratzler shear-force test. This technique, however, destroys the sample. Thus, there is need for a non-destructive and objective system to predict tenderness.

CHAPTER II

REVIEW OF LITERATURE

<u>Introduction</u>

Tenderness is a quality attribute of beef that is widely accepted as important. Smith et al. (1995) estimated an annual loss of \$250 million to the beef industry, due to lack of tenderness in beef cuts. Many tender and palatable carcasses have been discounted in value because of insufficient marbling. Yet sensory panel tests at the USDA Meat Animal Research Center indicate that marbling accounts for only 10% of the variation in beef ribeye tenderness (USDA, 1999).

Commercial packers have utilized several methods to improve tenderness in beef. Considerable research has been conducted on beef tenderness improvement. Packers generally employ methods like aging, special packaging, avoiding animal stress prior to slaughter, and electrical stunning. Nutritional methods, like incorporating vitamin D_3 in cattle feed (Berry et al., 2000) and genetic manipulation by biological engineering and selective breeding, are methods that have been researched to improve tenderness in beef. Plant derivatives, such as 'papain' from papaya, have been found to contain enzymes that increase tenderness. These enzymes are proteolytic in nature. Enzymes of the calpain system in the muscle, calpain I and calpain II, increase tenderness in beef by inducing proteolysis (Auburn University, 1996). They have a natural inhibitor known as calpastatin. Injection of calcium chloride in the carcass

6

(Whipple et al., 1992) and electrical stimulation (Ferguson et al., 2000) are two methods that have been found to increase the activity of the calpain system enzymes.

Historical Background

The importance of connective tissue in meat toughness has been a topic of debate among scientists (Swatland, 1995). They argue that characteristics like sarcomere length and integrity, and the state of the myofibrils and cytoskeleton are better indicators of beef toughness. Epley (2002) reported that aging the beef for a period of 11 days, while maintaining the temperature at - 1.1 to 1.6°C, gives the beef a "gamy" flavor and also increases tenderness. Reasons given for the increase in tenderness are changes that take place in the muscle fibers and the collagen, the latter being a major component of the connective tissue. Although the flavor increases as the aging period is prolonged, there is no increase in tenderness beyond 11 days of aging.

Minick et al. (2001) reported that steak samples with greater marbling were found to be more tender than those with less marbling. However, the test was performed on a small data set, and the correlation coefficient between shear force and marbling was a low - 0.26. Thus, there was no conclusive proof that there is strong correlation between tenderness and marbling.

The current industry accepted test for measuring tenderness is the Warner-Bratzler shear-force (WBS) test. The shear-force test is a standardized procedure recommended by the American Meat Science Association (AMSA, 1995). The WBS

test is assumed to simulate the chewing action of the teeth during the consumption of beef.

The shear-force test is a better alternative than testing for tenderness by a taste panel, because the latter introduces the element of subjective grading. An issue of concern is the fact that procedures for the WBS test have varied with application. Wheeler et al. (1997) suggested a set of procedures developed by Savell et al. (1994). One of the main reasons for the variation in procedures is the fact that consumers use different cooking methods, based on preference. Tenderness of the cooked beef varies with the method and the extent of cooking. Currently, a majority of the research institutions cook the meat to 71°C as required by the AMSA standard.

The WBS test procedure outlined in the AMSA (1995) standard is as follows:

1. Determine sample size based on appropriate statistical analysis or consult statisticians.
2. Remove primals from the carcasses no sooner than 24 h post mortem.
3. Time post-mortem for processing into cuts and freezing should be 14 days, including time for aging.
4. Thickness of the beef steaks should be 2.54 cm.
5. Steaks should be vacuum packaged or packaged in material with low oxygen permeability, and frozen to a temperature no higher than -18°C.
6. Steaks should be evaluated within 6 months of frozen storage time.
7. Thaw steaks until the internal temperature is 2-5°C.

8. Insert iron/constantan or copper/constantan thermocouple wires with a diameter less than 0.05 cm and error limits less than 2°C.

9. Roast or broil the steaks, as per recommended procedure, until the internal temperature is 71°C.

10. Chill the cooked samples overnight at 2-5°C or cool the samples (if they are not chilled) until they attain a uniform temperature between 24-28°C, prior to coring.

11. Obtain at least 6 cores from the samples, either manually or by machine drill coring, parallel to the longitudinal orientation of the muscle fibers. Cores should be 1.27 cm in diameter.

12. Shear each core once in the center using an Instron Universal Testing Machine, with a Warner-Bratzler shear head attachment. The crosshead speed of the machine should be 250 mm/min.

The disadvantages of the WBS test are that the procedure is destructive, much time and labor are involved, and the procedure is not suited for on-line evaluation. Scientists have sought out methods of detecting tenderness that would be non-destructive, time and labor efficient, and compatible with online evaluation.

Tenderness Probes

The Armour Tenderometer (AT) was one of the first developed probe systems (Belk et al., 2000). The system utilized a group of probes that predicted tenderness as a measure of the force required to penetrate the ribeye muscle. Huffman (1974)

reported an R^2 of 0.22 when the AT readings were correlated with WBS scores. No relationship was established between the AT readings and taste panel scores. Smith et al. (1984) reported a low correlation coefficient value of 0.10 (P<0.05) between the AT readings and taste panel scores. These studies concluded that the method was ineffective due to its inability to accurately predict tenderness.

The Meat Industry Research Institute of New Zealand (MIRINZ) developed a torsion-based tenderness probe. The instrument consists of two concentric sets of radially placed pins. The outer set of pins is static, while the inner set rotates. The meat is impaled on the pins, and the torque to the inner set of pins is generated by a synchronous motor. The torque and degree of rotation required to tear the meat are determined (Swatland, 1995). Jeremiah et al. (2000) evaluated the performance of the MIRINZ probe and reported that the probe was a faster alternative to WBS testing. However, the correlation coefficients for the relationships between the probe values and WBS scores, a trained sensory panel, and consumer ratings ranged from a low - 0.19 to - 0.26.

The Tendertec Mark III Beef Grading Instrument is a probe system developed by the Australian Meat Research Corporation to measure the amount of connective tissue and other factors contributing to meat toughness (Belk et al., 2000). The probe was a hand-held, battery-powered tenderometer (Swatland, 1995). The meat surface resistance to penetration of the needle in the probe was plotted as a function of depth. Belk et al. (2001) evaluated the effectiveness of the Australian Tendertec probe and

found significant correlation between the probe readings and other variables, i.e. WBS score, muscle fiber tenderness, overall tenderness, and amount of connective tissue. The variables; muscle fiber tenderness, overall tenderness, and amount of connective tissue were based on sensory panel scores. The probe, however, failed at sorting carcasses of young animals consistently, and the correlation coefficient declined for steaks as the degree of doneness increased. Higher correlation coefficient values were observed for steaks that were cooked to a rare or medium-rare degree of doneness. This study showed that the Tendertec probe had limited capacity to be used commercially.

The CT-probe or Connective Tissue probe is a prototype probe developed by the University of Guelph, Canada, supported by Ontario Cattlemen's Association and the Danish Meat Research Institute (Swatland et al., 1999). Functioning of the probe is based on ultra-violet fluorescence of the connective tissue. Most collagen types in meat have a peak excitation at 375 nm (Swatland, 1995). The CT-probe is hand-held, and has an optical window that penetrates the meat. This probe measures the whole band of the fluorescence emission spectrum against the depth of penetration of the probe. Peaks in the spectrum are recorded whenever the probe penetrates a layer of connective tissue. Damage to the carcass due to penetration is imperceptible. Swatland et al. (1998) evaluated the CT-probe for use in predicting taste and tenderness of broiled beef steaks. Samples were tested after aging periods of 3 days and 21 days. Probe readings were correlated with taste panel scores, with correlation coefficients ranging from 0.42 to 0.58.

Near-infrared (NIR) spectroscopy has been demonstrated to be a promising method for assessing meat quality, because it offers a non-invasive, and usefully accurate approach to predicting tenderness. Hildrum et al. (1995) studied the use of NIR reflectance spectroscopy in the prediction of sensory hardness, tenderness, and juiciness of bovine *Longissimus dorsi* muscles. For these three sensory features, principal component regression analysis of NIR reflectance data and sensory panel scores yielded correlation coefficients of 0.74, 0.70, and 0.61, respectively.

Park et al. (1998) used NIR reflectance spectra from a sample set of 119 steaks to predict WBS tenderness scores. Absorption was higher for extremely tough steaks, than for tender steaks. A partial least-square (PLS) model was developed to predict meat tenderness and a multi-linear regression (MLR) model was developed for meat tenderness classification. The PLS model yielded an R^2 value of 0.67 for the training set, and 0.63 for the validation set. The MLR model correctly classified 89% of the samples as "tender" or "tough."

Rodbotten et al. (2001) used NIR absorbance spectra to predict WBS scores. Two models were developed. The first model utilized the NIR spectra alone, and the second utilized NIR spectra in combination with information about post-slaughter treatments. Prediction models from NIR spectra alone gave correlation coefficients in the range of 0.52-0.83. When variables for post-slaughter treatments were included in the models, the correlation coefficients for predicting WBS scores were in the range

of 0.71-0.85. Based on these prediction models, the beef samples were classified into two tenderness groups. When classified into two groups, 73-98% of the samples were correctly classified.

Although the NIR approach shows promise, the technique has yet to be refined for on-line use at the processing plant. The fragile nature of a fiberglass NIR probe and its susceptibility to interfering light sources make the system precarious to use and prone to error.

Video Image Analysis

Video image analysis also offers a non-invasive approach to meat grading. One of the earliest efforts to develop an objective method of grading beef carcasses was carried out by the National Aeronautics and Space Administration (NASA). In 1978, NASA conducted research to determine the application of its technology to beef grading. They concluded that ultrasound and image analysis were the best available methods for automated and objective beef grading (Biju, 1998). The 1994 National Beef Instrument Assessment Plan (NBIAP) Symposium identified VIA systems, among the systems evaluated, as most promising for improving consistency and quality of beef (Wyle et al., 1999).

Belk (1999) reported that fat and lean color of beef muscle could indicate the ultra-structural status of the connective tissue. Tatum et al. (1997) reported a relation between calpastatin activity in the carcass and the lean color. Fiems et al. (2000) used

fat characteristics and lean color to predict tenderness in Belgian Blue bulls, using the Hunterlab Lab Scan-II. Lean color and fat characteristics both showed high correlation coefficient values, with respect to shear-force scores, ranging from 0.70-0.85.

Basset et al. (1999) proposed the use of texture analysis to classify images of meat slices. The selection of texture analysis was based on the ability of the human eye to discern various textures. First-order statistical features like the mean, and features based on second-order gray-level cooccurence matrices (GLCM) (Haralick et al., 1973) like correlation, entropy, and angular second moment were calculated. These features were extracted from the images in visible and ultraviolet (UV) portions of the spectrum. The features were correlated with dry-matter content, lipid content, collagen content, and four mechanical features. Correlation coefficients ranging from 0.1 to 0.67 were obtained for the classification. Basset et al. (1999) stated that texture analysis could be extended to prediction of tenderness in meat, because the meat tissue characteristics that influence meat quality, and the connective tissue quantity and spatial distribution that define the grain of meat are directly related to tenderness.

Li et al. (1999) utilized color features, marbling features, and image textural features for predicting beef tenderness. Mean, standard deviation, and skewness of the values of red-green-blue (RGB) components of the image, marbling features such as number of flecks and total area of the flecks, and image textural features such as pixel-value run length and pixel-value spatial dependence were extracted from the images. The

features were correlated with sensory panel scores. Color and marbling features were able to predict tenderness with an R^2 value of only 0.17. Color and marbling features were able to explain only 30% of the variation in tenderness. The inclusion of image textural features improved the R^2 to 0.62.

Basset et al. (2000) utilized the concept of ultraviolet fluorescence of collagen and image analysis to predict meat tenderness. In order to enhance the contrast between collagen and fat, images of the steaks were captured using both visible and UV light. Textural features based on the GLCM were used for predicting tenderness in meat. Gray-level cooccurence features, i.e., neighboring gray-level dependence matrix, gray-level run-length matrix, Fourier power spectrum, fractal method, and relative extrema measures, were correlated with the collagen content of the meat. A correlation coefficient of 0.49 was obtained.

Wyle et al. (1999) evaluated the performance of the HunterLab Video Imaging System, known popularly as BeefCam[TM], to predict WBS scores. The BeefCam[TM] is a self-contained, portable, handheld video-imaging unit that utilizes an internal mirror to reflect the image onto a horizontally positioned camera lens, while maintaining proper focal length. BeefCam[TM] operates, based on measurements of lean and fat color reflectance that are captured using VIA images containing up to 250,000 data points (pixels) per measurement. It can separate out different colors from irregularly shaped surfaces and be used to calculate relative areas that each color represents within the video image. Images are acquired in RGB color space and converted to

15

CIE L*, a*, and b* color space. The CIE L* a* b* color space is a perceptually uniform color space that simulates the functioning of the human eye. Wulf et al. (1997) correlated the values of CIE L* a* b* color space with both WBS scores and taste panel scores. The b* color band values showed the highest correlation. Correlation of b* values with WBS scores and taste panel scores was 0.38 and 0.37, respectively. Wyle et al. (1999) conducted two separate trials to predict tenderness and found that the BeefCam[TM] was able to correctly classify as "tender" or "tough", 150 out of 156 carcasses in the first trial and 139 of 150 carcasses in the second trial.

Using the Oklahoma State University VIA system, Jeyamkondan et al. (2001) explored textural features based on the GLCM to predict tenderness in meat. Instead of GLCM-based features, they chose to extract features derived from the gray-level difference histogram (GLDH). GLDH yields textural features similar to those based on GLCM, and offers the advantage of rapid computation. Seven textural features; energy, correlation, entropy, contrast, homogeneity, cluster shade, and cluster prominence were calculated in the RGB, CIE L* a* b*, and hue, saturation, and intensity (HSI) color spaces. Features were extracted from full and close-up images of the ribeyes. Textural features extracted from the full images predicted WBS scores with an R^2 value of 0.5 and correctly classified the steaks into categories of "tender" and "tough" with a 79% success rate. Features extracted from the close-up images predicted WBS scores with an R^2 value of 0.72 and classified the steaks with a 92% success rate. The close-up images produced better results, because they contained more detailed textural features than the full images.

Wavelet-based Textural Feature Analysis

Wavelets are mathematical functions that section data into separate frequency components and then address each component with resolution matched to its scale. They are superior to Fourier analysis methods in analyzing signals that are discontinuous and noisy. Wavelets have been utilized in the field of image and sound compression, de-noising signals, simulating human vision, earthquake predictions, etc.

Targeting beef quality grading, Kim et al. (1998) utilized the wavelet transform (WT) for multiresolutional texture analysis on ultrasound images of live cows. WT-based features included energy ratios, central moments of the decomposed sub-images, and wavelet edge density. Performance of the WT-based features was compared with GLCM-based features in predicting marbling distribution. The GLCM-based features predicted marbling distribution with a correlation coefficient of 0.58, whereas the WT-based features predicted with a value of 0.78. The WT-based features performed better, because they provided significant information about textural differences such as coarseness, orientation, and variations using spatial-scale localized texture information. These prediction models showed potential for objective quality grading using WT-based features.

Huang et al. (1997) utilized wavelet-based textural features for beef tenderness prediction. Ultrasonic elastogram images of beef samples were acquired for the study. GLCM-based features were extracted and compared with the WT-based features. The

WT-based textural features predicted WBS scores obtained after aging for 2, 14, 28, and 42 days with R^2 values ranging from 0.72-0.95. The R^2 value of prediction for the GLCM-based features ranged from 0.19 to 0.77. This study showed that WT-based features could make a unique contribution to beef tenderness prediction.

Li et al., (2001) utilized wavelet-based decomposition algorithms to extract textural features from images of beef samples. The images were transformed to the HSI color space from the standard RGB format. Textural features such as pixel-value run-length and primitive fraction were calculated from the decomposed images. Neural network and statistical models were used to compare the textural features with sensory panel scores. They achieved an 83.3% success rate classifying the beef samples into categories of "tender" and "tough."

The studies cited above indicate that there is potential for utilizing WT-based texture analysis for beef tenderness evaluation. The work conducted by Huang et al. (1997) reported high correlation between textural features and WBS scores. However, the study was conducted on ultrasound elastogram images taken from live cattle, and the sample size (n = 29) was too small to enable proper validation. Li et al. (2001) also reported a high success rate using wavelet-based texture analysis. However, they correlated the textural features with taste panel scores, rather than objective WBS scores.

Employing a sufficient sample size, this study will capture digital color images of beef steaks and extract textural features using computer analysis to predict beef tenderness.

Objectives

The overall objective of this study is to extend the Oklahoma State University VIA beef grading system to include prediction of tenderness. Specific objectives are to:

1. Develop image-processing algorithms to extract WT-based and GLDH-based textural features from steak ribeye images.

2. Develop statistical and neural network models to predict 14-day WBS tenderness scores using the image textural features.

3. Evaluate the performance of the algorithms in terms of the correlation of WBS scores with the textural features and the accuracy of classifying the steaks as "tender" and "tough."

4. Compare the ability of WT-based and GLDH-based features to predict beef tenderness.

CHAPTER III

MATERIALS AND METHODS

Overview

This chapter discusses the development and application of the VIA beef tenderness prediction system. The system consists of hardware components and supporting software. An algorithm was developed to extract WT-based textural features from images of beef steak ribeyes. Statistical and neural network models were developed. These models used the image textural features to predict WBS tenderness.

Hardware Components

The VIA system was comprised of a color video camera, a digitizer board, and a computer and monitor (Fig.1). Images of the steaks were captured by the camera. The digitizer converted the analog signal from the camera to digital format. Digital images were processed and analyzed by the computer.

Images of the beef steaks were captured in a diffuse lighting chamber (Fig. 2). The chamber consisted of a vaulted cover with a white interior to direct base lighting to a 20x30-cm imaging area (Fig. 3, Appen. B). Six 50-watt halogen lamps, powered by a stabilizing feedback controller, provided diffuse interior lighting. The camera was positioned on a graduated light stand equipped with a rack-and-pinion mount to raise or lower the camera. Steak samples were viewed through a circular viewing port in

the cover. Samples of beef steaks were placed on a removable pan and positioned in the viewing area beneath the camera. The pan had a black, non-reflective surface.
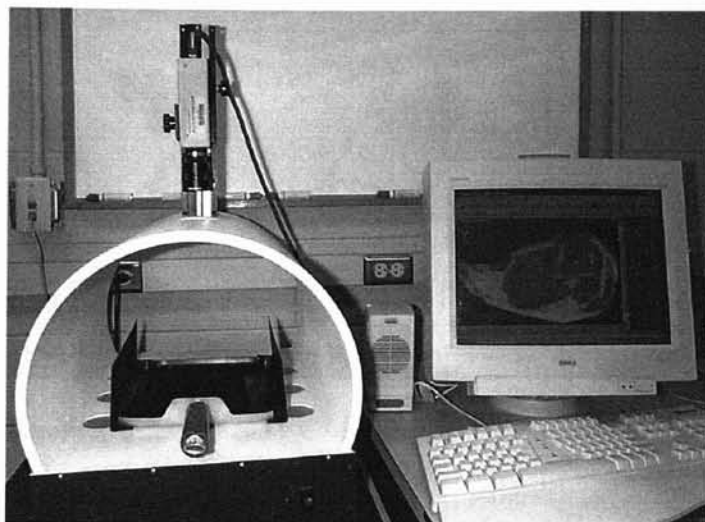
Figure1. Video image analysis system showing video camera, lighting chamber, positioning pan, and monitor.

A Microimage A209 RGB color video camera equipped with a 50-mm lens was used to acquire close-up images (Fig. 4). Fixing the F-stop between 5.6 and 8.0 prevented color saturation. The camera was set at a height of 46 cm above the surface of the beef steak ribeye.

An Integral Technologies Flashpoint 128 digitizer board was installed in a 1 GHz Dell Precision 420 computer equipped with 512 MB of RAM and a 40 GB hard disk.
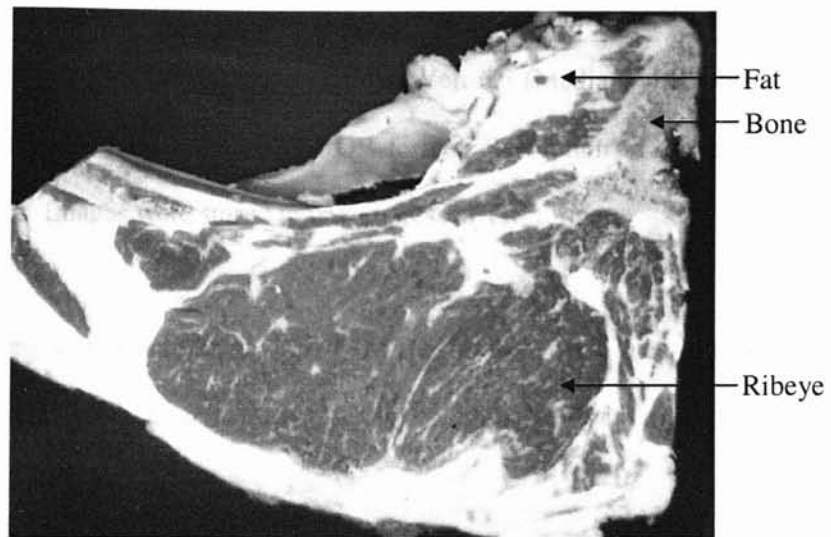
Figure 2. Image of sample beef steak.
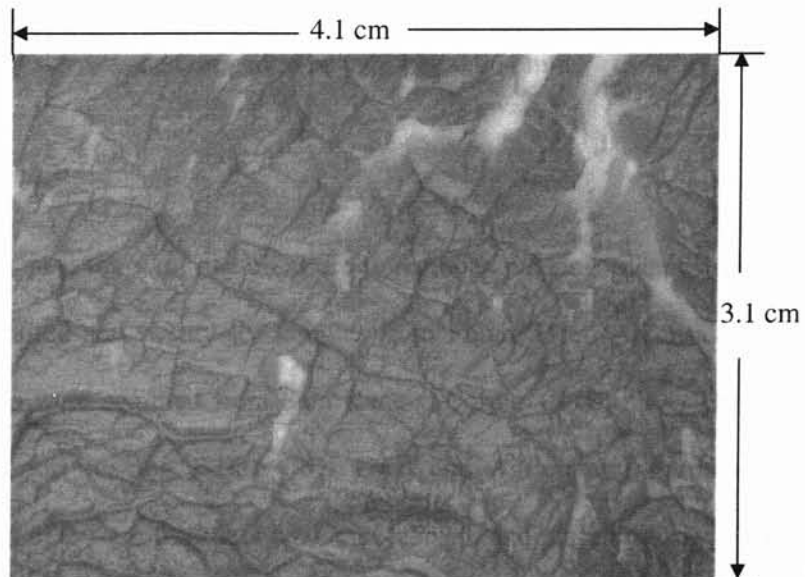
Figure 4. Close-up image of sample steak ribeye.

Software Components

Images were captured and stored using Optimas Ver. 6.5 (Media Cybernetics, Silver Spring, MD). Images were acquired in RGB format. Resolution of the images was 640 x 480 pixels. Images were stored in uncompressed TIF format.

Algorithms were written in Matlab Ver. 6.0 (The Math Works, Inc., Natick, MA). The software is coded in C and has toolboxes for applications in signal and image processing, including WT-based analysis.

Calibration

A calibration grid (Newport Corp.,1988) was used to relate the pixel size to measurable units. The grid, consisting of a 0.060-inch square mesh pattern, was placed beneath the camera. By calculating the number of squares on the captured image, the pixel size was determined to be 0.064 by 0.064 mm.

Samples

Steak samples (n=186) were acquired from regional packing plants during three visits. One-hundred and twenty-six samples from Future Beef, Arkansas City, KS, and 60 samples were acquired from Sam Kane's, Corpus Christi, TX. The samples were prepared for imaging at the OSU Food and Agricultural Products Center (FAPC). Steaks of 2.5-cm thickness were cut, labeled, and placed on trays. To allow for color to develop, steaks were 'bloomed' for a period of 30 minutes prior to imaging.

23

Shear-Force Measurement

Procedures recommended by AMSA (1995) were followed for measuring shear-force tenderness. After acquiring images, the steaks were vacuum packaged and aged for 14 days at 1°C. The steaks were then cooked in an impingement oven to an internal temperature of 70°C (Figs. 5 and 6). An impingement oven improves heat transfer by reducing the boundary-layer resistance through increased air velocity (Burrington, 1997). The result is a uniformly cooked sample. The cooked steaks were cooled and six 12-mm diameter core samples were removed from each ribeye. Each core was then sheared, perpendicular to the muscle fibers, in an Instron Universal Testing Machine fitted with a Warner-Bratzler shear-head attachment (Fig. 7). The mean of the peak shear-force values from six core samples was taken as the tenderness reference value. Higher values indicated "tougher" samples. Shear-force values exceeding 4.53 kg-force (kg-f) were defined as "tough" samples. Values below 4.53 kg-f were defined as "tender." Table I shows mean WBS scores (kg-f) for the samples, taken on 7th and 14th day of aging.

Shear-Force Measurement

Procedures recommended by AMSA (1995) were followed for measuring shear-force tenderness. After acquiring images, the steaks were vacuum packaged and aged for 14 days at 1°C. The steaks were then cooked in an impingement oven to an internal temperature of 70°C (Figs. 5 and 6). An impingement oven improves heat transfer by reducing the boundary-layer resistance through increased air velocity (Burrington, 1997). The result is a uniformly cooked sample. The cooked steaks were cooled and six 12-mm diameter core samples were removed from each ribeye. Each core was then sheared, perpendicular to the muscle fibers, in an Instron Universal Testing Machine fitted with a Warner-Bratzler shear-head attachment (Fig. 7). The mean of the peak shear-force values from six core samples was taken as the tenderness reference value. Higher values indicated "tougher" samples. Shear-force values exceeding 4.53 kg-force (kg-f) were defined as "tough" samples. Values below 4.53 kg-f were defined as "tender." Table I shows mean WBS scores (kg-f) for the samples, taken on 7th and 14th day of aging.

Figure 5. Steaks loaded into impingement oven.

Figure 6. Cooked steaks removed from the oven and
monitored for temperature.

all textural features share is that they express spatial interactions between the pixels of an image neighborhood (Van de Wouwer et. al., 1999).

Textural features are often random in nature. Numerous attempts at modeling texture have included random field modeling, cooccurence matrices, and spatial-frequency techniques. Thus, no single best texture model has been defined.

Textural features contain both spatial and frequency information. The raw signal is a time-domain or temporal representation. This representation is not the most useful, because it gives no information regarding the frequency content.

According to Heisenberg's uncertainty principle, the position and momentum of a moving particle cannot be known simultaneously at a given instant (Polikar, 2002). This principle also applies to signal and image processing. Frequency and spatial information of a signal cannot be determined simultaneously.

The Fourier transform (FT) is a mathematical function that determines the frequency content of the signal (Polikar, 2002). The FT analyzes the signal, globally. The frequency spectrum shows what frequencies exist in a signal, and the amplitude represents the frequency content. Digital images are spatial representations. The FT of an image yields a spatial frequency spectrum in which the high-frequency components are depicted in the center, and the low-frequency components are represented toward the outside. The FT is a global representation of the signal.

The short-time Fourier transform (STFT) analyzes the signal, locally. The signal is divided into small and equal segments, within which the signal is assumed to be stationary. A window function is used to separate the signal into equal segments. However, the length of the window is fixed for a given representation. Choice of a window function is based on the nature of application. A wider window gives good frequency resolution, but poor spatial resolution. Narrower windows give poor frequency resolution, but good spatial resolution. Thus, choosing a window presents a challenge when the need arises to select an optimum window length for the whole signal.

Wavelet Transform

The wavelet transform (WT) overcomes the shortcomings of the STFT by using a variable-length window. A variable-length window is able to represent low-frequency components by using a wider window, and high-frequency components with a smaller window.

Evaluation according to scale is the principle behind wavelet analysis. Scale is defined as 1/frequency. The scale parameter in the wavelet analysis is similar to the scale used in maps. High-scale maps provide a global view, and thus provide low-frequency information. Low-scale maps give a more detailed view, and thus provide information of high intricacy or high frequency.

The analytical approach utilized in WT is termed multiresolution analysis (MRA). This procedure implies that the signal is analyzed at different frequencies with different resolutions (Polikar, 2002). MRA is designed to give good spatial resolution and poor frequency resolution at high frequencies, while yielding good frequency resolution and poor spatial resolution at low frequencies. Thus, the MRA approach is best suited when a given signal has high-frequency components for short durations and low-frequency components for longer durations. Fortunately, most signals encountered in practical applications follow this pattern.

The continuous wavelet transform (CWT) is similar to the STFT in the sense that a window function is multiplied by the signal, and the transform is computed separately for different segments of the spatial-domain signal. However, the transform computed using the CWT is not an FT. Wavelets are compactly supported functions of finite width. In contrast, an FT has cosine- and sine-based functions that are of infinite width. In wavelet transformation, negative frequencies of a sinusoidal signal are not computed, and thus a single peak corresponds to a sinusoid.

In the WT, a prototype function called an analyzing wavelet or 'mother' wavelet, is adopted. The mother wavelet is a prototype for generating other window functions. All the windows used are dilated or compressed and shifted versions of the mother wavelet. Spatial analysis is performed on a contracted, high-frequency version of the prototype, while frequency analysis is done on a dilated, low-frequency version. The

wavelet functions of the prototype can be truncated or modified according to requirements.

The continuous one-dimension wavelet transform of a signal $f(x)$ is defined by Livens et al. (1997), as:

$$(W_a f)\ (b) = \int f(x)\ \psi^*_{a,b}\ (x)\ dx,\qquad(1)$$

where: $\psi_{a,b}$ is computed from the mother wavelet, ψ, by translation and dilation, given by:

$$\psi_{a,b}\ (x) = \frac{1}{\sqrt{a}}\ \psi\ \frac{(x-b)}{a}\qquad(2)$$

where: a = translation parameter, measure of time

b = scale parameter, 1/frequency.

The Haar wavelet is the simplest of all mother wavelets. It is a square step-function. Other types of wavelets are termed biorthogonal, Daubechies, Mexican hat, Morlets, symlets, and coiflets.

Discretizing the CWT or making the CWT mathematically discrete, offers a feasible computational approach. Solving the FT, STFT, or CWT by hand, using integrals and equations, is not practical. These computations require the use of computers, and hence, the need to discretize the transforms.

30

The Nyquist theorem states that the highest frequency that can be accurately represented is less than one-half of the sampling rate. In other words, the sampling frequency should be twice that of the original frequency. This rule is followed in order to prevent aliasing.

A variable-resolution tool such as WT can be utilized to discretize the signal by varying the sampling rate. At higher scales or lower frequencies, the sampling rate can be reduced. This operation can be represented by the equation:

$$N_2 = S_2 \frac{N_1}{S_1} \tag{3}$$

where: S_1 and S_2 = scales for the sampling rates of N_1 and N_2.

The discretized CWT is merely a sampled version of the CWT. The sampled version still contains redundant information, which increases computation time (Polikar, 2002). This redundancy is of concern where reconstruction or synthesis of the signal is required.

The discrete wavelet transform (DWT) provides sufficient information both for analysis and synthesis of the raw signal. In the discrete case, filters of different cut-off frequencies are used to analyze the signal at different scales. The signal is passed through a series of high-pass filters to analyze the high frequencies and passed through a series of low-pass filters to analyze the low frequencies. The filtering

process changes the resolution of the signal, whereas subsampling or upsampling operations change the scale. Filter implementation of the DWT is shown in Figure 8, Appendix B.

An important property of the DWT is the relationship between the impulse responses of the low-pass and high-pass filters. The relationship is given by:

$$g[L-1-n] = (-1)^n \, h[n] \tag{4}$$

where: $g[n]$ = high-pass filter

$h[n]$ = low-pass filter

L = filter length.

These filters are known as quadrature mirror filters (QMF), because each filter is an odd-index alternated, reversed version of the other. Conversion into the other type of filter is brought about by the $(-1)^n$ term.

The raw signal is passed through the filter banks that are comprised of low- and high-pass filters. Approximation coefficients of the signal are obtained through the low-pass filter, whereas the high-pass filter gives detailed coefficients. After the filtering, half of the samples can be eliminated according to Nyquist's rule, since the signal now has a highest frequency of $\pi/2$ radians, instead of π. This process of upsampling and subsampling, along with the filtering operations is known as decomposition.

The amount of subsampling increases as the number of levels of decomposition increases. The higher-frequency components are extracted with higher resolution at the first level of decomposition. As the levels of decomposition increase, low-frequency components are extracted at lower resolution. Due to successive subsampling by 2, the signal length must be a power of 2, or at least a multiple of a power of 2, in order for this scheme to be efficient. Length of the signal determines the number of levels to which the signal can be decomposed. For example, if the signal length is 1024, ten levels of decomposition are possible (Polikar, 2002).

Wavelet Decomposition of Images

The two-dimensional (2-D) WT is the result of filtering by the product of two one-dimensional (1-D) wavelet transforms. Wavelet decomposition of a 2-D image can be obtained by performing the filtering operations consecutively in the horizontal and vertical directions (Livens et al., 1997). Rows of the input image are passed through the low- and high- pass filter bank, followed by subsampling by a factor of 2. Columns of the resulting images from the filter bank are filtered further by low- and high-pass filters. This sequence of filtering is followed by subsampling by a factor of 2. The entire process represents a single level of decomposition.

Each level of decomposition yields four subimages, namely; approximation, horizontal, vertical, and diagonal. The approximation subimage consists of high-frequency components of the original image. Horizontal, vertical, and diagonal subimages consist of low-frequency components. Decomposed images can be viewed

33

by reconstructing the coefficients of the subimages at each level. Since every subimage is subsampled by a factor of 2, there is complete reconstruction. This procedure leads to a representation with the same number of pixels as the original image.

Wavelet image decomposition provides a representation that is easy to interpret. Every subimage has conveniently separated information of specific scale and orientation. Spatial information is retained within the images (Livens et al., 1997).

Wavelet-based Textural Features

Coefficients of a detailed subimage resulting from wavelet decomposition sum to zero. It is therefore necessary to compute a non-linear function of the coefficients in order to obtain textural features. The most commonly used function is the square, which gives the energy of the subimage when summed. Wavelet energy signatures indicate the distribution of energy of a subimage along the frequency axis, with respect to scale and orientation. Wavelet energy signatures have proven to be very useful for gray-level texture characterization (Van de Wouwer et al., 1999).

Van de Wouwer et al. (1999) define energy of a subimage as:

$$E_{ni} = \int (D_{ni}(\vec{b}))^2 \, d\vec{b} \tag{5}$$

where: D_{ni} = directional detail information at a given scale, n.

The most straightforward extension of energy signatures to color images is to transform each color space separately and extract the energies of each transformed plane. The number of features will be tripled, because they are extracted in a tristimulus plane such as RGB, HSI, or CIE L* a* b* color spaces. RGB and CIE L* a* b* color spaces were utilized for extracting features in this study.

The images were decomposed using Haar and Daubechies wavelets up to five levels of decomposition. Since the decomposition is performed by a factor of 2, the maximum allowable decomposition was five, using images with a resolution of 640 by 480 pixels.

Wavelet transform operations were performed separately in the RGB and CIE L* a* b* color spaces. Both Haar and Daubechies wavelets were used for decomposing the images. Subimages at the 5th level of decomposition showed highly detailed features (Fig. 9, Appen. B). This characteristic enabled the extraction of highly detailed textural features at the higher levels of decomposition.

The first trial involved WT operations on regular images. The second trial involved contrast stretching of the images prior to WT operations. Contrast stretching (often called normalization) is a simple image enhancement technique that attempts to improve the contrast in an image by 'stretching' the range of intensity values it contains to span a desired range of values, e.g., the full range of pixel values allowed by the type of image involved (University of Edinburgh, 2002). One method to

35

enhance contrast of an image by contrast stretching is histogram equalization. Histogram equalization is a non-linear, monotonic mapping method that re-assigns the intensity values of pixels in the input image to achieve a uniform distribution of intensities in the output image. In this study, contrast stretching was conducted by finding limits or pairs of intensities to increase contrast of an image. These limits were then used to adjust the image intensity values, or colormap.

Wavelet textural features were obtained for both the regular and contrast-stretched images in each color band of the RGB and CIE L* a* b* color spaces. The features were extracted after reconstructing the subimages from the coefficients. These features were:

1. Energy signatures

2. Energy ratios

3. Variance

4. Skewness

5. Kurtosis

6. Wavelet edge density.

Energy of the subimages was calculated using Eq. (5). Energy ratios between the levels of decomposition were calculated separately for the approximation, horizontal, vertical, and diagonal subimages. These ratios were computed to compare the amount of energy in each directional subimage (Kim et al., 1998).

Central moments of the pixel values, including variance (second moment), skewness (third moment), and kurtosis (fourth moment) were also calculated from the reconstructed subimages. Skewness values for the detailed subimages (horizontal, vertical, and diagonal) were very low and, thus, were not calculated in further simulations.

Wavelet edge density measures the coarseness or smoothness of texture (Kim et al., 1998). Edges of the decomposed subimages were enhanced by replacing the low-frequency components of the subimages with zero, thus emphasizing the high-frequency components. After reconstruction the subimages, energy was calculated using Eq. (5) to estimate the edge density.

Gray-Level Cooccurence Matrix Textural Features

The concept of gray-level cooccurence matrices was proposed by Haralick et al. (1973) to extract second-order textural features from images. The concept was based on the spatial distribution of the gray levels. The proposed 14 textural features depended on the ability to capture textural information in a matrix containing relative frequencies by which a gray-level 'i' occurs with a neighboring gray-level 'j', separated by a distance 'd' and gray-level orientation. Features such as contrast, correlation, energy, entropy, etc., were proposed for gray-level orientations of 0°, 45°, 90°, and 135°. Unser (1986) proposed the gray-level difference histogram (GLDH) as an alternative to the computationally intensive GLCM. Sum images were constructed by adding the value of a given pixel to the neighboring pixel values. Difference

images were constructed by subtracting the value of a given pixel from the neighboring pixels.

For this study, six GLDH features were calculated from the reconstructed subimages with distance of 1 pixel and an angle of 0°. Distance of 1 pixel was selected to reveal fine textural details. Initially, four angles (0, 45, 90, and 135°) were used to extract the textural features. Because the textures were uniform on the images of the steaks, all angles yielded similar features. Therefore, only the angle of 0° was used in this study. The GLDH-based features were as follows:

1. Contrast

2. Entropy

3. Homogeneity

4. Correlation

5. Cluster Shade

6. Cluster Prominence.

Performance of the WT-based textural features and GLCM-based features were compared.

Feature Reduction

A problem in WT-based textural analysis is redundancy, which occurs when the textural features are extracted in tristimulus color spaces such as RGB, CIE L* a* b*, or HSI. A large number of textural features are derived from each subimage, which

makes classification very difficult. One method of reducing the number of redundant features is normalizing. This method is a post-generation operation, i.e., performed after the features have been extracted.

In this project, post-generation feature reduction was achieved by using linear regression to obtain the best features from each color space and from regular and contrast-stretched images. These features were then combined, and principal component analysis (PCA) was performed on these combined features to further reduce redundancy. This analysis transforms the input data so that the elements of the input vectors will be uncorrelated. In addition, the size of the input vectors may be reduced by retaining only those components that contribute more than a specified fraction of the total variation in the data set. Before conducting PCA, the textural features were standardized to have zero mean and unit variance. The number of principal components selected explained 99% of the variation of the original features. Both, GLDH- and WT- based features, were reduced and normalized separately for analysis.

Statistical Analysis

Stepwise regression analysis techniques were used to predict 14th day postmortem average WBS scores. Samples were separated into two sets; training and test. Training and test sets were formed using random number generation. The ratio of sample sizes between the training and test sets was 3:1. The training and test sets consisted of 137 samples and 49 samples, respectively. Use of the random approach

for forming test and training sets removed human bias. Both training and test data sets included a truncated data set, which gave the best fits when predicting WBS scores. This truncated data set was obtained by linear regression, described earlier in relation to feature reduction.

The truncated set of features was evaluated by stepwise regression to obtain the regression equation and correlation coefficient for predicting WBS tenderness scores. The training set alone was used to find the regression equation and report the correlation coefficient values.

Procedures described by Wheeler et al. (2002) were then implemented for evaluation of the VIA system. This procedure was considered better able to analyze the project sample set, which was deficient in number and range of "tough" samples in our data. This judgement is corroborated in following paragraphs.

Wheeler et al. (2002) assessed performance of three instrumented tenderness prediction systems on the basis of progressive certification of steak sample "tenderness" in 10% certification increments. In their procedure, WBS scores predicted by linear regression, were sorted in ascending order. Values of WBS scores less than 4.53 kg-f (10 lb-f) were certified "tender", and values equal to or greater than 4.53 kg-f were certified "tough." Based on the sorted, ascending order of the predicted WBS scores, actual WBS scores were sorted. Assuming that the model performed as desired, the actual WBS scores would also be sorted in ascending order.

A 10% certification level implied that 10% of the steak samples having the lowest predicted WBS scores were classified into a "certified tender" category, and the rest into a "not certified tender" category. Mean observed WBS scores from these two categories were compared using a t-test for independent samples at a significance level of 0.05 (α=0.05). Satterthwaite approximation was used to estimate variance, when the variances of the two categories were not equal. If the variances were equal, a pooled variance estimate was used in the t-test.

This procedure was repeated in 10% increments up to a 100% certification level. A significant difference in mean observed shear force values between the two groups indicated that the VIA system had successfully sorted the "tender" from the "tough" samples at that certification level.

The data set (n=186) used for this project contained only 10 tough samples, constituting only 5.4% percent of the total. As mentioned earlier, if the samples were sorted properly based on the ascending order of WBS scores, the training and test sets should consist of only "tender" samples up to the 90% certification level.

Descriptive statistics for WT- and GLDH-based textural features, for both training and test sets, are shown below in Tables II and III.

Table II: Descriptive statistics of shear-force values for training and test data sets for WT-based textural features

Data Set	N	Range	Mean (kg-f)	SD (kg-f)	> 4.53 kg-f
Training	137	2.25-5.81	3.39	0.65	7
Test	49	2.39-4.81	3.46	0.60	3

Table III: Descriptive statistics of shear-force values for training and test data sets for GLDH-based textural features

Data Set	N	Range	Mean (kg-f)	SD (kg-f)	> 4.53 kg-f
Training	137	2.25-5.21	3.35	0.62	7
Test	49	2.30-5.81	3.56	0.69	3

It can be inferred from the mean values of the WBS scores that the samples in the data set were predominantly "tender." Due to the lack of sufficient "tough" samples, a confusion matrix could not be plotted to estimate the accuracy of prediction. The t-test suggested by Wheeler et al. (2002) was a better option because it could separate the "tough" samples and contain them in the 100% certification level.

Statistical analysis was performed using SAS Ver. 8.1 (SAS World Headquarters, Cary, NC).

Neural Network Analysis

Artificial neural networks (ANN) are one of the widely used techniques in data mining and machine learning. Modeled on the functioning of the human brain, an ANN is comprised of interconnected nodes arranged in layers. The ANN has an

activation function and a learning rule to map the input to the output by adjusting the input weights and bias. The adjustment is based on the input pattern.

The backpropagation neural network (BPNN) is a multi-layer perceptron. Backpropagation was created by generalizing the Widrow-Hoff learning rule, or delta learning rule, to multi-layer networks and nonlinear differentiable transfer functions (Demuth et al., 1998). Widrow-Hoff learning is an approximate steepest-descent algorithm, in which the performance index is the mean square error (MSE) between the predicted and targeted values (Hagan et al., 1996). The learning rule is a supervised operation occurring in each cycle or 'epoch' through a forward flow of outputs and a backward propagation of the error resulting from the adjustment of weights. The first layer has weights coming from the input. Each subsequent layer has a weight coming from the previous layer. All layers have bias. The last layer is the network output. The transfer functions can be any differentiable transfer function such as hyperbolic tangent sigmoid, log-sigmoid, or linear. Details regarding transfer functions can be found in Hagan et al. (1996).

The performance function for a backpropagation neural network is the MSE, which is the same as that for Widrow-Hoff learning. This performance function does not prevent the use of large weights and bias that can lead to overfitting and poor performance of the network. The performance function given by Demuth et al. (1998) prevents the use of larger weights and bias. As a result, the network response is

smoother and less likely to overfit. The performance function is represented in the given equation as:

$$F = MSE + (1-\gamma)\ MSW \tag{6}$$

where: F = performance function

MSE = mean square error between output and target values

γ = regularization parameter

MSW = mean square of network weights and biases.

BPNN was employed using the following training functions:

1. Quasi-Newton algorithm

2. Levenberg-Marquardt algorithm

3. Variable learning rate

4. Resilient backpropagation

5. Bayesian regularization.

Newton's method is based on the second-order Taylor series expansion (Hagan et al., 1996). The basic step of Newton's method is given by the equation below:

$$x_{k+1} = x_k - A_k^{-1} * g_k \tag{7}$$

where: A_k = Hessian matrix or second derivative of the performance index

g_k = gradient or first derivative of the function.

Quasi-Newton methods belong to a class of algorithms that are based on Newton's methods, but don't require the tedious calculation of the Hessian matrix. Instead, an approximation of the Hessian matrix is updated during each iteration of the algorithm (Demuth et al., 1998).

The Levenberg-Marquardt algorithm is similar to quasi-Newton methods in that it involves second-order training, without calculating the Hessian matrix. The approximation used for the Hessian matrix by this algorithm is given by:

$$x_{k+1} = x_k - [J^T J + \mu I]^{-1} J^T e \tag{8}$$

where: J = Jacobian matrix that contains derivatives of network errors

e = vector of network errors

μ = scalar function, with adjustable values to speed up or improve the performance function.

Variable learning rate is an improvement on the steepest-descent algorithm, that uses a constant learning rate. Large values of the learning rate will speed up the convergence, but cause oscillations and instability during training. Small values of the learning rate stabilize the algorithm, but lengthen the time to converge. Instead, performance of the algorithm is improved by varying the learning rate during training. An adaptive learning rate attempts to keep the learning step size as large as possible, without subjecting the algorithm to instability or oscillation.

Resilient backpropagation is another improvement of the steepest-descent algorithm that resembles the variable learning rate algorithm. Networks that employ sigmoid transfer functions require that the slope of the transfer function approach zero as the input size increases. When steepest-descent algorithms are used to train, convergence is very slow. This effect occurs because the magnitude of gradient is very small, causing small changes in weights and bias (Demuth et al., 1998). Resilient backpropagation training utilizes only the sign of the gradient to determine the direction of weight update. The size of the weight change is determined by a separate function. Weight size is increased when the sign does not change after two successive iterations and decreases when the sign changes from the previous iteration.

The Bayesian regularization algorithm is a network training function that updates the weights and bias values according to Levenberg-Marquardt optimization. Weights and biases of the network are assumed to be random variables with specified distributions. The algorithm minimizes a combination of squared errors and weights, and then determines the correct combination so as to produce a network that generalizes well (Demuth et al., 1998). More details regarding Bayesian regularization techniques can be found in Mackay (1992).

In this project, the BPNN was trained using all five training functions, separately. Results of each of the training functions were evaluated separately, based on network

stability and value of the correlation coefficient. Neural network analysis was performed using Matlab Ver. 6.0.

CHAPTER IV

RESULTS AND DISCUSSION

A sample set of beef steaks (n=186), were imaged for tenderness evaluation by the VIA system. Statistical and neural network models were developed from textural features to predict shear-force tenderness values. Success of the model was based on the prediction correlation coefficient and on the accuracy of classifying steaks as "tender" or "tough."

Statistical Analysis Results

Truncated WT- and GLDH-based textural features were analyzed separately in two sets by stepwise linear regression. Both sets contained features derived from Haar and Daubechies decomposition. This truncated set of features did not contain information from contrast-stretched images, thus confirming that contrast stretching did not improve performance of the model. The significance level for the features to be entered and remain in the stepwise regression model was 0.15 ($\alpha = 0.15$).

Results from the preliminary stepwise regression analysis showed that WT-based textural features predicted the 14th day postmortem WBS tenderness with a correlation coefficient value of 0.57. GLDH-based textures predicted WBS tenderness with a correlation coefficient of 0.48. Both Haar and Daubechies wavelets contributed equally in predicting tenderness. Among the features extracted from the

detailed subimages, those from the approximation subimages contributed least to prediction of WBS tenderness. Regression equations derived from the training set were used to predict WBS scores in the training and test sets.

For both WT- and GLDH-based features, the training and the test set contained seven and three "tough" samples, respectively. The training set of the WT-based features had two misclassified samples at the 80% and 90% "certified tender" levels. No errors were found up to the 70% level. In the test set, one "tough" sample was misclassified at the 80% level (signified by the asterisk in Table IV, Appendix A). At all certification levels for both training and test sets, there were significant differences between the means of the shear-force values for "certified tender" and "not certified tender" samples.

In the training set for GLDH-based features, two "tough" samples were incorrectly classified at the 80% "certified tender" level. There were no errors up to the 70% level. The test set had one misclassified "tough" sample at the 90% level (signified by the asterisk in Table V, Appendix A), and had no errors up to the 80% level. At all certification levels for the training set, there were significant differences between means of the shear force values for "certified tender" and "not certified tender" samples. However, in the test set, at the 10% and the 70% certification levels (signified by asterisk in Tables VI and VII), there were no significant differences between means of the shear-force values of the two groups. Tables V and VI are given on the following page.

Table VI: Statistical differences of mean shear-force values between "certified tender" and "not certified tender" groups for WT-Based textural features

Percentage Certified	Training Set (n=137)			Test Set (n=49)		
	Certified Tender	Not Certified Tender	Difference	Certified Tender	Not Certified Tender	Difference
90	3.2876	4.2872	0.9996	3.4076	3.9636	0.5560
80	3.2439	3.9839	0.7400	3.3279	3.9968	0.6689
70	3.1911	3.8716	0.6805	3.2382	3.9771	0.7389
60	3.1296	3.7896	0.6600	3.2528	3.7712	0.5184
50	3.1271	3.6563	0.5292	3.2250	3.6942	0.4692
40	3.0732	3.6021	0.5289	3.1609	3.6566	0.4957
30	2.9773	3.5721	0.5948	3.0514	3.6296	0.5782
20	2.9391	3.5055	0.5660	2.9891	3.5862	0.5969
10	2.7684	3.4605	0.6920	2.8674	3.5322	0.6650

Table VII: Statistical differences of mean shear-force values between "certified tender" and "not certified tender" groups for GLDH-based textural features

Percentage Certified	Training Set (n=137)			Test Set (n=49)		
	Certified Tender	Not Certified Tender	Difference	Certified Tender	Not Certified Tender	Difference
90	3.2914	4.1715	0.8801	3.4729	3.6261	0.1532
80	3.2297	3.9737	0.7440	3.4523	3.6430	0.1910
70	3.2054	3.7679	0.5630	3.4207	3.7091	0.3064*
60	3.1644	3.6974	0.5330	3.3122	3.7665	0.4543
50	3.1676	3.5938	0.4262	3.2253	3.7588	0.5335
40	3.0760	3.5825	0.5065	3.1548	3.7130	0.5582
30	2.9953	3.5493	0.5540	3.1192	3.6615	0.5423
20	3.0347	3.4687	0.4340	3.1169	3.5908	0.4739
10	3.0115	3.4224	0.4109	3.0144	3.5476	0.5332*

* Mean observed shear force values for "certified tender" and "not certified tender" were not significantly different at $\alpha = 0.05$.

Neural Network Analysis Results

The BPNN model consisted of two hidden layers. The first hidden layer had ten neurons with a log-sigmoid transfer function, and the second hidden layer had twenty neurons with a tangent sigmoid transfer function. The output layer had one neuron with a linear transfer function.

The truncated GLDH- and WT-based features were analyzed separately. Both data sets contained features derived from Haar and Daubechies wavelet decomposition. As mentioned earlier, features obtained from contrast-stretched images were not present in the two sets.

Prior to feeding the textural features into the network, the input vectors were normalized. Normalization was followed by PCA to remove redundant features. The number of principal components selected explained 99% of the variation of the original features. After preliminary analysis, the input vectors were split into training and test sets. Based on sample size, the ratio between the training and test data sets was 3:1.

Of the five training functions used, Bayesian regularization provided equal or near equal correlation coefficient values for the training and test sets. The Bayesian-based network was trained for 25 to 30 epochs. The MSE remained constant after training the network for 20 epochs, so no further training was performed in order to avoid overfitting. Networks utilizing the other four training functions were trained for

higher numbers of epochs. However, they performed poorly in predicting WBS tenderness, despite the substantial reduction in MSE. The correlation coefficient in the training and test sets varied considerably. Correlation coefficient values for the training set ranged from 0.75 to 1.0. For the test set, values ranged from 0.35 to 0.56. The large difference in the correlation coefficient values between the test and training sets indicated that none of the four training functions was able to stabilize the network.

For WT-based textural features, correlation between the observed WBS and predicted values for both training and test data sets ranged from 0.57 to 0.59. GLDH-based textural features predicted WBS tenderness with correlation coefficients of 0.55 and 0.31 for training and test data sets, respectively. It can be inferred from the correlation coefficients that WT-based textural features were able to predict WBS scores more accurately than GLDH-based features. Training and test sets of the WT-based features gave nearly similar values of correlation coefficients, indicating that the network was more stable working with WT-based features, than with GLDH-based features.

Results of the statistical and neural network analysis indicated that WT-based features predicted WBS scores better than GLDH-based features. The analyses also showed that features derived from contrast-stretched images did not contribute to predicting WBS scores.

Conclusions

The OSU VIA system was extended to extract textural features from the ribeye images and create models to predict meat tenderness, with moderate success. The results indicated that WT-based features were better predictors of WBS tenderness than GLDH-based features, on the basis of correlation coefficients and results of the statistical t-test. The t-test indicated that 71.4% and 66.7% of "tough" samples in the training and test set, respectively, were successfully sorted from the "tender" samples. However, the correlation coefficients for predicting WBS tenderness scores were very low. There were also errors in classification of "certified tender" and "not certified tender" at two certification levels in the t-test. These discrepancies are probably magnified by the following data conditions:

1. The data were highly skewed towards the "tender" side. Only ten "tough" samples, approximately 5.4%, were included in the entire set of 186 samples. This distribution lacked the balance needed to formulate an effective statistical or neural network model.

2. The WBS data obtained from the Department of Animal Science Meat Laboratory was not entirely reliable. Many samples showed an increase in WBS scores on the 14th day of aging when compared with scores taken on the 7th day (Indicated by asterisk, Table I, Appen. A). Since aging is found to increase tenderness up to the 11th day, these data contradicted the established pattern.

53

Despite the anomalies in the data, both WT- and GLDH-based textural feature models were able to establish a moderate correlation between the textural features and WBS tenderness, and the *t*-test was able to sort the "tender" and "tough" samples with acceptable accuracy.

Further Research

The goal of including tenderness prediction in the USDA quality grading procedures is a major task. The OSU system demonstrated the use of textural features extracted from images of fresh steaks to predict cooked-beef tenderness and the ability to sort steaks on the basis of cooked tenderness. Hence, this project has shown that VIA systems offer an objective, efficient, and non-destructive method for predicting tenderness in meat. Several modifications to the VIA system might improve results. Suggestions for further research are listed below:

1. Having a greater number of "tough" samples in the data set should give the model better balance in predicting tenderness. Therefore, samples from mature animals, or those not subjected to artificial tenderizing procedures, should be included in the data set.

2. Frequency-domain features derived from Fourier transforms should be explored for extracting textural features. Directionality and coarseness features of a Fourier power spectrum could yield information regarding tenderness.

3. Despite the fact that extent of marbling features has been found to explain only 10% of variation beef tenderness, there is a possibility that marbling features, combined with other textural features and color scores, could enrich data related to tenderness. Scores for lean maturity could also be incorporated.

4. NIR analysis has shown promise for tenderness prediction and classification. Application is hampered by difficulty in implementing for on-line use. This drawback might be corrected by employing cameras that cover a sufficient portion of the NIR spectrum.

5. Extracting textural features in the UV spectrum is another worthy approach to tenderness prediction. UV light causes collagen to fluoresce. Since one of the factors associated with meat toughness is the collagen in the connective tissue, this approach could quantify the relationship between collagen and tenderness.

Among the suggested approaches, I see the most promise in NIR and UV technology. These two methods could objectively identify contributors to meat tenderness, due to their ability to scan in a spectral range invisible to the human eye. In time, a well established and approved tenderness rating for beef carcasses will be developed to add value to the product and optimize consumer satisfaction.

REFERENCES

AMSA. 1995. Research guidelines for cookery, sensory evaluation and instrumental tenderness measurements of fresh meat. Chicago, IL; American Meat Science Association, National Live Stock and Meat Board.

Auburn University. 1996. AU researcher seeking ways to improve tenderness of meats. Auburn University News. http://www.auburn.edu/administration/univrel/news/archive/1_96news/1_96autenderness.html.

Basset, O., F. Dupont, A. Hernandez, C. Odet, S. Abouelkaram, and J. Culioli. 1999. Texture image analysis: Application to the classification of bovine muscles from meat slice images. *Optical Engineering* 38(11). 1950-1959.

Basset, O., B. Buquet, S. Abouelkaram, P. Delachartre, and J. Culioli. 2000. Application of texture image analysis for the classification of bovine meat. *Food Chemistry* 69(2000): 437-445.

Belk, K.E.. 1999. Techniques to identify palatable beef carcasses: HunterLab BeefCam^{TM}. *Proceedings of the Range Beef Cow Symposium* XVI, Greely, CO.

Belk, K.E. M.H. George, J.D. Tatum, G.G. Hilton, R.K. Miller, M. Koohmaraie, J.O. Reagen, and G.C. Smith. 2001. Evaluation of the Tendertec beef grading instrument to predict the tenderness of steaks from beef carcasses. *Journal of Animal Science* 79: 688-697.

Belk, K.E., J. A. Scanga, A. M. Wyle, and G. C. Smith. 2000. Prediction of beef palatability using instruments. Beef Improvement Federation Convention, Wichita, KS. http://ansci.colostate.edu/ran/meat/klb001.pdf. Accessed August 8, 2002.

Berry, B.A., D.R. Gill and R. Ball. 2000. Effects of feeding vitamin D on feedlot performance, carcass traits, and meat tenderness of finishing steers. OSU 2000 Animal Science Research Report: 98-103. http://www.ansi.okstate.edu/research/2000rr/19.htm. Accessed August 8, 2002.

Biju, N.1998. Beef quality grading with color video image analysis. MS Thesis, Oklahoma State University, Stillwater, OK.

Burrington, K.J.. 1997. Out of the frying pan. http://www.foodproductdesign.com/archive/1997/0997DE.html.

Demuth, H., and M. Beale. 1998. Neural network toolbox for use with Matlab®-User's Guide. Version 3. Natick, MA: The Mathworks, Inc..

Epley, R.J. 2002. Aging Beef. http://www.extension.umn.edu/distribution/nutrition/DJ5968.html. Accessed on August 9, 2002.

Ferguson D.M., A. Egan, D. Perry, and J. Thompson. 2000. CRC Annual Report 1999/2000. New South Wales, Australia. The Cooperative Research Centre for Cattle and Beef Quality.

Fiems L.O., S. De Campeneere, S. De Smet, G. Van de Voorde, J.M. Vanacker, and C. V. Boucqué. 2000. Relationship between the fat depots in carcasses of beef bulls and effect on meat colour and tenderness. *Meat Science* 56 (2000): 41-47.

Hagan, M., H. Demuth, and M. Beale. 1996. Neural Network Design. Boston, MA: PWS Publishing.

Haralick, R.M., K. Shanmugam, and I. Dinstein. 1973. Textural features for image classification. *IEEE Transactions on Systems, Man, and Cybernetics* SMC-3(6):610-621.

Hildrum, K.I., T. Isaksson, T. Naes, B.N. Nilsen, M. Rodbotten, and P. Lea. 1995. Near infrared reflectance spectroscopy in the prediction of sensory properties of beef. *Journal of Near Infrared Spectroscopy* 3: 81–87.

Huang, Y., R.E. Lacey, L.L. Moore, R.K. Miller, A.D. Whittaker, and J. Ophir.1997. Wavelet textural features from ultrasonic elastograms for meat quality prediction. *Transactions of the ASAE* 40(6): 1741-1748.

Huffman, D.L. 1974. An evaluation of the Tenderometer for measuring beef tenderness. *Journal of Animal Science* 38:287-294.

Jeremiah, L.E. and D.M. Phillips. 2000. Evaluation of a probe for predicting beef tenderness. *Meat Science* 55(2000): 493-502.

Jeyamkondan, S., N. Ray, G. A. Kranzler, and N. Biju. 2000. Beef quality grading using machine vision. Proceedings of SPIE, Volume 4203: 91-101.

Jeyamkondan, S., G.A. Kranzler, and A. Lakshmikanth. 2001. Predicting beef tenderness with computer vision. *ASAE Paper No. 013063*. St. Joseph, Michigan: ASAE.

Kim, N., V. Amin, D. Wilson, G. Rouse, and S. Udpa. 1998. Ultrasound image texture analysis for characterizing intramuscular fat content of live beef cattle. *Ultrasonic Imaging* 20: 191-205.

Koohmaraie, M., T. L. Wheeler, and S. D. Shackelford. 2002.Beef tenderness: Regulation and prediction. USDA-ARS. http://meats.marc.usda.gov/MRUWWW/ TENDREV/TEN DREV.html. Accessed May 29, 2002.

Kranzler, G.A. and H.G.Dolezal. 1998. Color video image analysis for augmenting beef carcass grading. Final report: Food Technology Center Research Initiative Program.

Li, J., J. Tan, F.A.Martz and H. Heymann.1999. Image texture features as indicators of beef tenderness. *Meat Science* 53(1999): 17-22.

Li, J., J. Tan, and P. Shatadal. 2001. Classification of tough and tender beef by image texture analysis. *Meat Science* 57(2001): 341-346.

Livens, S., P. Scheunders, G. Van de Wouver, and D. Van Dyck. 1997. Wavelets for texture analysis: An overview. 6th Int. Conf. on image processing and its applications: 581-585. Dublin, Ireland.

MacKay, D. J. C. 1992. Bayesian interpolation. *Neural Computation* 4(3): 415-447.

Minick, J.A., D.E. Wilson, and J.R. Strohbehn. 2001. Preliminary analysis of data from the Iowa beef tenderness and carcass evaluation project. http://www.extension. iastate.edu/Pages/ansci/beefreports/asl1739.pdf. Accessed on August 9, 2002.

Newport Corporation. 1988. Machine vision optics guide. Fountain Valley, CA.

NCBA. 2002. http://www.beef.org/dsp/dsp_locationContent.cfm?locationId=28. Accessed on August 2, 2002.

OBIC. 2002. http://www.oklabeef.org/Beeffacts/beeffactsstarter.htm. Accessed on August 2, 2002.

Park, B., Y.R. Chen, W.R. Hruschka, S.D. Shackelford , and M. Koohmaraie. 1998. Near-Infrared reflectance analysis for predicting beef longissimus tenderness. *Journal of Animal Science* 76: 2115-2120.

Polikar, R. 2002. The wavelet tutorial. College of Engineering, Rowan University. http://www.public.iastate.edu/~rpolikar/WAVELETS/waveletindex.html. Accessed on August 29, 2002.

Rodbotten, R., Mevik, B-H, and Hildrum. K.I. 2001. Prediction and classification of tenderness in beef from non-invasive diode-array detected NIR spectra. *Journal of Near Infrared Spectroscopy* 9: 199–210.

Samal, A.2002. Medical Image Analysis- Course Powerpoint Handouts. Department of Computer Science and Electrical Engineering, University of Nebraska, Lincoln.

http://csce.unl.edu/~samal/class/Sum02/496/handouts/Texture.ppt. Accessed on August 29, 2002.

Savell, J., R. Miller, T. Wheeler, M. Koohmaraie, S. Shackelford, B. Morgan, C. Calkins, M. Miller, M. Dikeman, F. McKeith, G. Dolezal, B. Henning, J. Busboom, R. West, F. Parrish, and S.Williams. 1994. Standardized Warner-Bratzler shear force procedures for genetic evaluation. http//savell-j.tamu.edu/shearstand.html. Accessed on August 2, 2002.

Smith, G.C. Z. L. Carpenter, H.R. Cross, G.E. Murphey, H.C. Abraham, J.W. Savell, G.W. Davis, B.W. Berry and F.C. Parrish, Jr. 1984. Relationship of USDA marbling groups to palatability of cooked beef. *Journal of Food Quality* 7:289-308.

Smith, J.C., J.W. Savell, H.G. Dolezal, T.G. Field, D.R. Gill, D.B. Griffin, D.S. Hale, J.B. Morgan, S.N. Northcutt and J.D. Tatum. 1995. National Beef Quality Audit-1995. Conducted by Colorado State University, Texas A&M University, and Oklahoma State University for National Beef Cattlemen's Association: 270.

Schutte, B., N. Biju, G.A. Kranzler, and H.G. Dolezal. 1998. Color video image analysis for augmenting beef carcass grading. OSU 1998 Animal Science Research Report:32-36. http://www.ansi.okstate.edu/research/1998rr/07.html. Accessed on August 2, 2002.

Swatland, H.J. 1995. On-line evaluation of meat. Lancaster, PA: Technomic Publishing Company Incorporated.

Swatland, H.J., J.C. Brooks, and M.F. Miller. 1998. Possibilities for predicting taste and tenderness of broiled beef steaks using an optical-electromechanical probe. *Meat Science* Vol. 50 No.1: 1-12.

Swatland, H.J. and C.J. Findlay. 1999. Testing the CT- Probe for meat toughness on commericially competitive sources of beef. Ontario Beef Research Update. http://131.104.112.18/beefupdate/articles96/a-testing_the_ct.htm. Accessed August 14, 2002.

Tatum, J.D., M.H. George, K.E. Belk, and G.C. Smith. 1997. Development of a palatability assurance "critical control points" (PACCP) model to reduce the incidence of beef palatability problems. Final Report to the National Cattlemen's Beef Association. Colorado State University, Fort Collins.

University of Edinburgh. 2002. Image processing learning resources. http://www.dai.ed.ac.uk /HIPR2/stretch.htm. Accessed September 2, 2002.

Unser, M..1986. Sum and difference histograms for texture classification. *IEEE Transactions on Pattern Analysis and Machine Intelligence,* Vol. PAMI-8 No. 1: 118-125.

USDA. 1999. Predicting Tenderness in Beefsteaks. Agricultural Research Magazine. http://www.ars.usda.gov/is/AR/archive/nov99/beef1199.htm. Accessed August 8, 2002.

Van de Wouwer, G., P. Scheunders, S. Livens and D. Van Dyck. 1999. Wavelet correlation signatures for color texture characterization. *Pattern Recognition* 32(3): 443-451.

Wheeler, T.L., S.D. Shackelford, L.P. Johnson, M.F. Miller, R.K. Miller and M. Koohmaraie. 1997. A comparison of Warner-Bratzler shear force assessment within and among institutions. *Journal of Animal Science* 75:2423-2432.

Wheeler, T,L., D. Vote, J.M. Leheska, S.D. Shackelford, K.E. Belk, D.M. Wulf, B.M. Gwartney, and M. Koohmaraie. 2002. The efficacy of three objective systems for identifying guaranteed tender beef cuts. Accepted for publication in *Journal of Animal Science*.

Whipple, G., and M. Koohmaraie. 1992. Freezing and calcium chloride marination effects on beef tenderness and calpastatin activity. *Journal of Animal Science.* 70: 3081-3085.

Wulf, D. M., S. F. O'Connor, J. D. Tatum, and G. C. Smith. 1997. Using objective measures of muscle color to predict beef longissimus tenderness. *Journal of Animal Science* 75: 684-692.

Wyle, A.M., R.C. Cannell, K.E. Belk, M. Goldberg, R. Riffle, and G.C. Smith. 1999. An evaluation of the prototype portable HunterLab video imaging system (BeefCam) as a tool to predict tenderness of beef carcasses using objective measures of lean and fat color. *1999 Beef Program Report.* Department of Animal Sciences, Colorado State University.

APPENDICES

APPENDIX A- STATISTICAL TABLES

Table I: Mean WBS scores for samples taken on 7th and 14th
day of aging

Sample ID	Harvest Date	Day 7 Mean (kg-f)	Day 14 Mean (kg-f)	Shear Force Difference
OBIC 1	1/11/02	3.539	2.818	0.721
OBIC 2	1/11/02	3.088	2.250	0.838
OBIC 3	1/11/02	2.824	2.650	0.173
OBIC 4	1/11/02	3.529	3.182	0.347
OBIC 5	1/11/02	3.073	2.729	0.344
OBIC 6	1/11/02	3.973	2.824	1.150
OBIC 7	1/11/02	5.256	3.139	2.117
OBIC 8	1/11/02	3.235	2.440	0.795
OBIC 9	1/11/02	5.918	3.558	2.361
OBIC 10	1/11/02	4.278	4.196	0.083
OBIC 11	1/11/02	3.062	2.730	0.332
OBIC 12	1/11/02	3.645	3.306	0.339
OBIC 13	1/11/02	3.591	3.071	0.520
OBIC 14	1/11/02	2.678	2.608	0.070
OBIC 15	1/11/02	3.747	3.310	0.437
OBIC 16	1/11/02	3.392	2.677	0.715
OBIC 17	1/11/02	2.738	3.743	-1.006*
OBIC 18	1/11/02	2.550	3.101	-0.551*
OBIC 19	1/11/02	2.741	3.315	-0.574*
OBIC 20	1/11/02	3.108	3.648	-0.540*
OBIC 21	1/11/02	3.436	3.239	0.197
OBIC 22	1/11/02	3.103	3.047	0.056
OBIC 23	1/11/02	3.374	2.459	0.915
OBIC 24	1/11/02	3.198	2.552	0.647
OBIC 25	1/11/02	2.934	2.682	0.252
OBIC 26	1/11/02	2.707	2.696	0.011
OBIC 27	1/11/02	3.468	2.447	1.021
OBIC 28	1/11/02	2.880	2.988	-0.108*
OBIC 29	1/11/02	2.962	2.392	0.570
OBIC 30	1/11/02	3.154	3.837	-0.682*
OBIC 31	1/11/02	2.860	2.601	0.260
OBIC 32	1/11/02	4.580	3.873	0.707
OBIC 33	1/11/02	2.736	2.689	0.048
OBIC 34	1/11/02	3.854	3.440	0.414
OBIC 35	1/11/02	3.700	3.623	0.077
OBIC 36	1/11/02	2.824	2.596	0.228
OBIC 37	1/11/02	5.547	3.309	2.238
OBIC 38	1/11/02	3.401	3.004	0.397
OBIC 39	1/11/02	3.850	3.067	0.783
OBIC 40	1/11/02	5.705	4.816	0.890
OBIC 41	1/11/02	3.960	3.507	0.453
OBIC 42	1/11/02	4.574	4.163	0.411
OBIC 43	1/11/02	4.676	3.797	0.879
OBIC 44	1/11/02	3.804	2.893	0.912
OBIC 45	1/11/02	3.270	2.908	0.362
OBIC 46	1/11/02	7.157	4.163	2.994
OBIC 47	1/11/02	3.549	2.646	0.904
OBIC 48	1/11/02	3.840	2.830	1.011
OBIC 49	1/11/02	4.231	3.744	0.486
OBIC 50	1/11/02	2.977	3.013	-0.036*
OBIC 51	1/11/02	3.703	3.613	0.090
OBIC 52	1/11/02	3.517	3.620	-0.103
OBIC 53	1/11/02	3.472	3.307	0.165
OBIC 54	1/11/02	3.660	2.870	0.790
OBIC 55	1/11/02	4.225	3.057	1.167
OBIC 56	1/11/02	3.876	2.380	1.496
OBIC 57	1/11/02	4.866	3.527	1.339
OBIC 58	1/11/02	3.447	3.359	0.088
OBIC 59	1/11/02	5.166	4.392	0.774
OBIC 60	1/11/02	4.205	4.482	-0.278*
OBIC 61	1/11/02	3.778	3.910	-0.132*

OBIC 62	1/11/02	2.935	2.894	0.041
OBIC 63	1/11/02	4.692	4.044	0.648
OBIC 64	1/11/02	4.125	3.401	0.724
OBIC 65	1/11/02	3.261	2.821	0.439
OBIC 66	1/11/02	3.635	3.253	0.382
OBIC 67	1/11/02	4.949	3.686	1.263
OBIC 68	1/11/02	4.201	4.129	0.072
OBIC 69	1/11/02	3.340	3.306	0.034
OBIC 70	1/11/02	5.758	5.809	-0.051*
OBIC 71	1/11/02	3.467	3.112	0.354
OBIC 72	1/11/02	2.827	2.767	0.061
OBIC 73	1/11/02	4.162	2.984	1.177
OBIC 74	1/11/02	3.054	3.682	-0.628*
OBIC 75	1/11/02	3.482	2.915	0.567
OBIC 76	1/11/02	3.568	3.678	-0.111*
OBIC 77	1/11/02	5.037	3.939	1.098
OBIC 78	1/11/02	5.561	3.769	1.792
OBIC 79	2/13/02	4.488	3.315	1.173
OBIC 80	2/13/02	2.935	2.856	0.079
OBIC 81	2/13/02	3.562	2.805	0.757
OBIC 82	2/13/02	3.729	2.943	0.786
OBIC 83	2/13/02	3.789	2.845	0.944
OBIC 84	2/13/02	3.399	3.864	-0.465*
OBIC 85	2/13/02	4.291	3.926	0.365
OBIC 86	2/13/02	3.293	3.447	-0.154*
OBIC 87	2/13/02	3.470	2.989	0.480
OBIC 88	2/13/02	3.404	3.353	0.051
OBIC 89	2/13/02	2.934	2.674	0.260
OBIC 90	2/13/02	3.210	3.384	-0.175*
OBIC 91	2/13/02	2.902	3.056	-0.154*
OBIC 92	2/13/02	3.514	4.068	-0.554*
OBIC 93	2/13/02	2.899	2.690	0.210
OBIC 94	2/13/02	3.887	2.686	1.201
OBIC 95	2/13/02	2.787	3.948	-1.161*
OBIC 96	2/13/02	3.471	3.257	0.214
OBIC 97	2/13/02	4.001	3.018	0.983
OBIC 98	2/13/02	2.497	2.303	0.194
OBIC 99	2/13/02	2.871	3.106	-0.235*
OBIC 100	2/13/02	3.176	3.189	-0.013*
OBIC 101	2/13/02	3.751	3.211	0.540
OBIC 102	2/13/02	3.584	3.619	-0.034*
OBIC 103	2/13/02	3.953	2.957	0.996
OBIC 104	2/13/02	3.499	3.365	0.135
OBIC 105	2/13/02	3.197	3.126	0.070
OBIC 106	2/13/02	3.826	3.635	0.191
OBIC 107	2/13/02	3.212	3.802	-0.590*
OBIC 108	2/13/02	3.494	3.221	0.273
OBIC 109	2/13/02	3.783	3.268	0.516
OBIC 110	2/13/02	4.978	3.058	1.920
OBIC 111	2/13/02	5.204	4.483	0.721
OBIC 112	2/13/02	4.038	2.737	1.301
OBIC 113	2/13/02	3.126	4.140	-1.014*
OBIC 114	2/13/02	3.302	3.143	0.159
OBIC 115	2/13/02	2.783	3.714	-0.931*
OBIC 116	2/13/02	4.288	5.213	-0.924*
OBIC 117	2/13/02	3.263	2.951	0.312
OBIC 118	2/13/02	2.874	2.959	-0.086*
OBIC 119	2/13/02	3.382	3.558	-0.176*
OBIC 120	2/13/02	4.993	3.306	1.687
OBIC 121	2/13/02	2.918	3.648	-0.729*
OBIC 122	2/13/02	2.851	2.489	0.362
OBIC 123	2/13/02	3.648	4.122	-0.474*
OBIC 124	2/13/02	2.796	3.168	-0.372*
OBIC 125	2/13/02	3.278	2.509	0.769
OBIC 126	2/13/02	4.896	3.452	1.444
OBIC 127	1/15/02	3.736	4.299	-0.563*

64

OBIC 128	1/15/02	4.278	2.639	1.639
OBIC 129	1/15/02	4.753	4.302	0.451
OBIC 130	1/15/02	3.308	2.591	0.717
OBIC 131	1/15/02	4.455	3.112	1.343
OBIC 132	1/15/02	3.987	4.173	-0.186*
OBIC 133	1/15/02	2.962	3.509	-0.547*
OBIC 134	1/15/02	4.964	3.157	1.807
OBIC 135	1/15/02	4.992	4.792	0.199
OBIC 136	1/15/02	4.464	2.987	1.477
OBIC 137	1/15/02	3.770	3.204	0.566
OBIC 138	1/15/02	4.709	4.332	0.377
OBIC 139	1/15/02	4.710	3.086	1.623
OBIC 140	1/15/02	5.796	5.167	0.629
OBIC 141	1/15/02	4.037	2.783	1.254
OBIC 142	1/15/02	4.263	3.478	0.784
OBIC 143	1/15/02	3.342	3.243	0.099
OBIC 144	1/15/02	4.771	3.369	1.402
OBIC 145	1/15/02	4.077	3.777	0.300
OBIC 146	1/15/02	5.032	5.159	-0.127*
OBIC 147	1/15/02	3.722	3.483	0.239
OBIC 148	1/15/02	3.803	4.047	-0.244*
OBIC 149	1/15/02	5.104	2.480	2.624
OBIC 150	1/15/02	4.146	3.609	0.537
OBIC 151	1/15/02	3.048	3.951	-0.903*
OBIC 152	1/15/02	3.247	4.208	-0.961*
OBIC 153	1/15/02	2.958	2.953	0.005
OBIC 154	1/15/02	3.990	3.698	0.292
OBIC 155	1/15/02	3.535	3.493	0.041
OBIC 156	1/15/02	3.717	3.527	0.189
OBIC 157	1/15/02	3.764	3.370	0.394
OBIC 158	1/15/02	3.366	3.058	0.308
OBIC 159	1/15/02	3.692	3.829	-0.137*
OBIC 160	1/15/02	3.251	4.156	-0.906*
OBIC 161	1/15/02	4.435	3.892	0.543
OBIC 162	1/15/02	3.593	2.951	0.642
OBIC 163	1/15/02	3.089	3.293	-0.204*
OBIC 164	1/15/02	3.438	3.173	0.265
OBIC 165	1/15/02	5.197	4.613	0.584
OBIC 166	1/15/02	3.927	3.699	0.229
OBIC 167	1/15/02	3.304	3.425	-0.121*
OBIC 168	1/15/02	4.536	3.772	0.765
OBIC 169	1/15/02	3.335	2.958	0.377
OBIC 170	1/15/02	4.160	3.890	0.270
OBIC 171	1/15/02	4.280	4.332	-0.052*
OBIC 172	1/15/02	3.333	3.337	-0.004*
OBIC 173	1/15/02	3.907	3.916	-0.010*
OBIC 174	1/15/02	3.853	3.250	0.603
OBIC 175	1/15/02	4.273	3.174	1.099
OBIC 176	1/15/02	3.884	3.221	0.663
OBIC 177	1/15/02	5.197	4.341	0.855
OBIC 178	1/15/02	4.629	3.924	0.706
OBIC 179	1/15/02	3.490	3.317	0.174
OBIC 180	1/15/02	4.381	4.667	-0.286*
OBIC 181	1/15/02	4.951	5.079	-0.128*
OBIC 182	1/15/02	4.096	3.666	0.430
OBIC 183	1/15/02	4.252	3.079	1.173
OBIC 184	1/15/02	3.211	3.658	-0.446*
OBIC 185	1/15/02	4.964	4.226	0.739
OBIC 186	1/15/02	4.242	4.689	-0.447*

* Suspect WBS reading, indicating decrease in tenderness with
  increase in aging period.

Table V: Samples sorted based on predicted scores with certification levels for GLDH-based textural features (test set)

Sample ID	Predicted Scores (kg-f)	Actual Scores (kg-f)	Tender/Tough Categories	Certification Levels
OBIC 17	3.073	3.743	Tender	
OBIC 10	3.104	4.196	Tender	
OBIC 98	3.139	2.303	Tender	10%
OBIC 50	3.141	3.013	Tender	
OBIC 15	3.154	3.310	Tender	
OBIC 125	3.197	2.509	Tender	
OBIC 43	3.201	3.797	Tender	
OBIC 63	3.207	4.044	Tender	20%
OBIC 14	3.212	2.608	Tender	
OBIC 7	3.214	3.139	Tender	
OBIC 94	3.218	2.686	Tender	
OBIC 16	3.219	2.677	Tender	
OBIC 176	3.232	3.221	Tender	30%
OBIC 167	3.233	3.425	Tender	
OBIC 74	3.234	3.682	Tender	
OBIC 88	3.279	3.353	Tender	
OBIC 53	3.282	3.307	Tender	
OBIC 11	3.308	2.730	Tender	40%
OBIC 147	3.331	3.482	Tender	
OBIC 106	3.360	3.635	Tender	
OBIC 75	3.362	2.914	Tender	
OBIC 13	3.364	3.071	Tender	50%
OBIC 156	3.399	3.527	Tender	
OBIC 49	3.399	3.744	Tender	
OBIC 42	3.401	4.163	Tender	
OBIC 54	3.415	2.870	Tender	
OBIC 60	3.418	4.482	Tender	60%
OBIC 104	3.425	3.364	Tender	
OBIC 78	3.434	3.769	Tender	
OBIC 97	3.447	3.018	Tender	
OBIC 59	3.456	4.392	Tender	
OBIC 134	3.465	3.157	Tender	70%
OBIC 41	3.473	3.507	Tender	
OBIC 68	3.484	4.129	Tender	
OBIC 127	3.511	4.299	Tender	
OBIC 32	3.530	3.873	Tender	
OBIC 175	3.541	3.174	Tender	80%
OBIC 30	3.571	3.837	Tender	
OBIC 159	3.583	3.829	Tender	
OBIC 144	3.637	3.369	Tender	
OBIC 111	3.645	4.483	Tender	
OBIC 40	3.649	4.816	Tough*	90%
OBIC 77	3.680	3.939	Tender	
OBIC 51	3.688	3.613	Tender	
OBIC 132	3.696	4.173	Tender	
OBIC 110	3.728	3.058	Tender	
OBIC 89	3.829	2.674	Tender	100%
OBIC 70	3.841	5.809	Tough	
OBIC 180	3.879	4.667	Tough	

*Misclassified "tough" sample at the indicated certification level

Table V: Samples sorted based on predicted scores with certification levels for GLDH-based textural features (test set)

Sample ID	Predicted Scores (kg-f)	Actual Scores (kg-f)	Tender/Tough Categories	Certification Levels
OBIC 17	3.073	3.743	Tender	
OBIC 10	3.104	4.196	Tender	
OBIC 98	3.139	2.303	Tender	10%
OBIC 50	3.141	3.013	Tender	
OBIC 15	3.154	3.310	Tender	
OBIC 125	3.197	2.509	Tender	
OBIC 43	3.201	3.797	Tender	
OBIC 63	3.207	4.044	Tender	20%
OBIC 14	3.212	2.608	Tender	
OBIC 7	3.214	3.139	Tender	
OBIC 94	3.218	2.686	Tender	
OBIC 16	3.219	2.677	Tender	
OBIC 176	3.232	3.221	Tender	30%
OBIC 167	3.233	3.425	Tender	
OBIC 74	3.234	3.682	Tender	
OBIC 88	3.279	3.353	Tender	
OBIC 53	3.282	3.307	Tender	
OBIC 11	3.308	2.730	Tender	40%
OBIC 147	3.331	3.482	Tender	
OBIC 106	3.360	3.635	Tender	
OBIC 75	3.362	2.914	Tender	
OBIC 13	3.364	3.071	Tender	50%
OBIC 156	3.399	3.527	Tender	
OBIC 49	3.399	3.744	Tender	
OBIC 42	3.401	4.163	Tender	
OBIC 54	3.415	2.870	Tender	
OBIC 60	3.418	4.482	Tender	60%
OBIC 104	3.425	3.364	Tender	
OBIC 78	3.434	3.769	Tender	
OBIC 97	3.447	3.018	Tender	
OBIC 59	3.456	4.392	Tender	
OBIC 134	3.465	3.157	Tender	70%
OBIC 41	3.473	3.507	Tender	
OBIC 68	3.484	4.129	Tender	
OBIC 127	3.511	4.299	Tender	
OBIC 32	3.530	3.873	Tender	
OBIC 175	3.541	3.174	Tender	80%
OBIC 30	3.571	3.837	Tender	
OBIC 159	3.583	3.829	Tender	
OBIC 144	3.637	3.369	Tender	
OBIC 111	3.645	4.483	Tender	
OBIC 40	3.649	4.816	Tough*	90%
OBIC 77	3.680	3.939	Tender	
OBIC 51	3.688	3.613	Tender	
OBIC 132	3.696	4.173	Tender	
OBIC 110	3.728	3.058	Tender	
OBIC 89	3.829	2.674	Tender	100%
OBIC 70	3.841	5.809	Tough	
OBIC 180	3.879	4.667	Tough	

*Misclassified "tough" sample at the indicated certification level

APPENDIX B- FIGURES
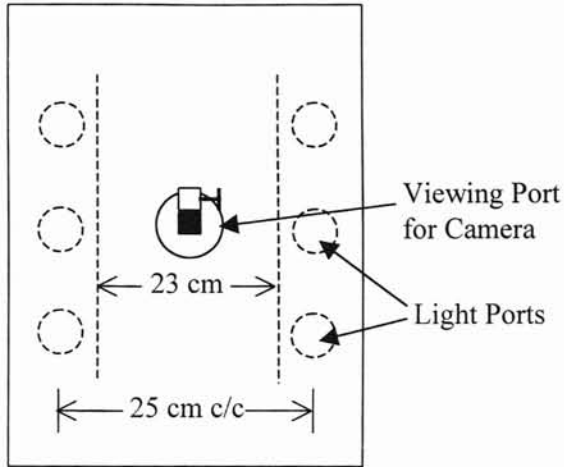
TOP VIEW
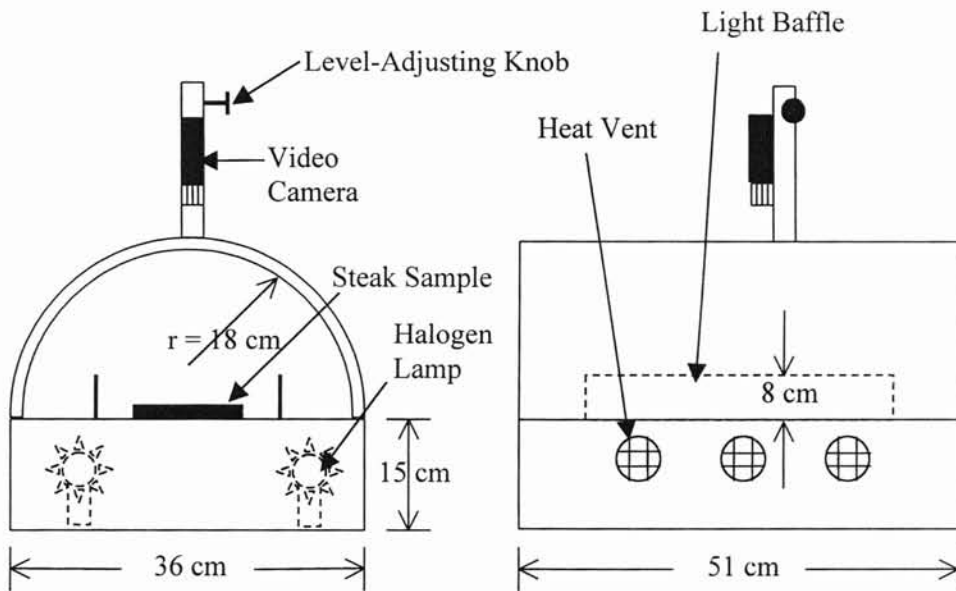
FRONT VIEW   **SIDE VIEW**

Figure 3. Lighting chamber detail.

69
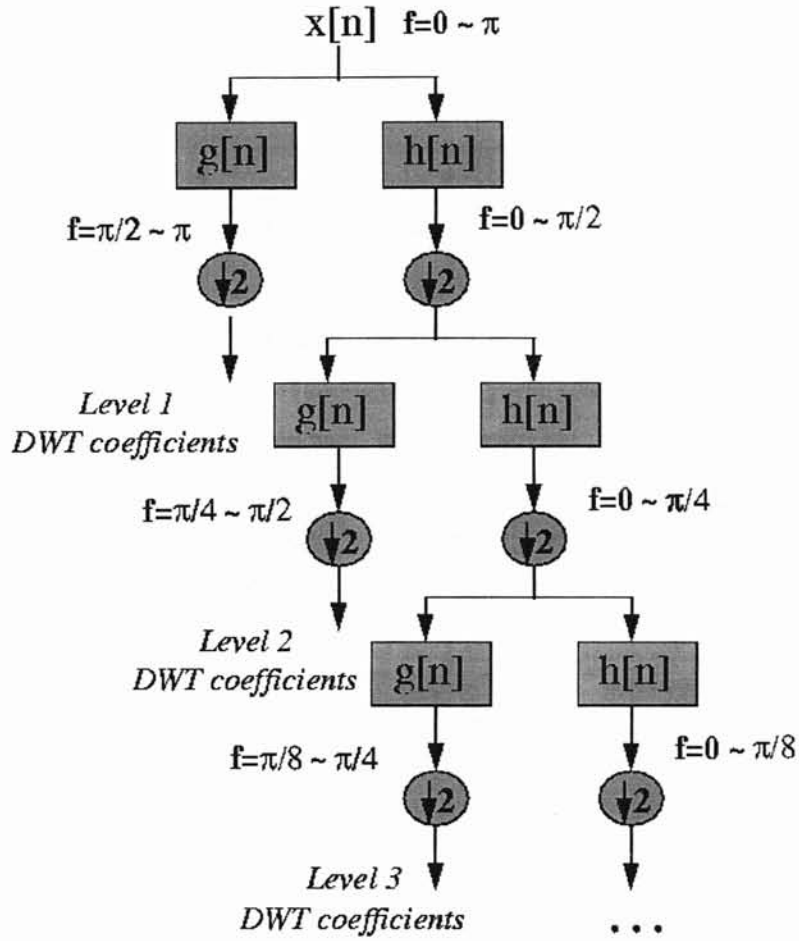
Figure 8. Filter implementation of the discrete wavelet transform
(Pollikar, 2002). g[n]: high-pass filter, h[n]: low-pass filter.

Original Image
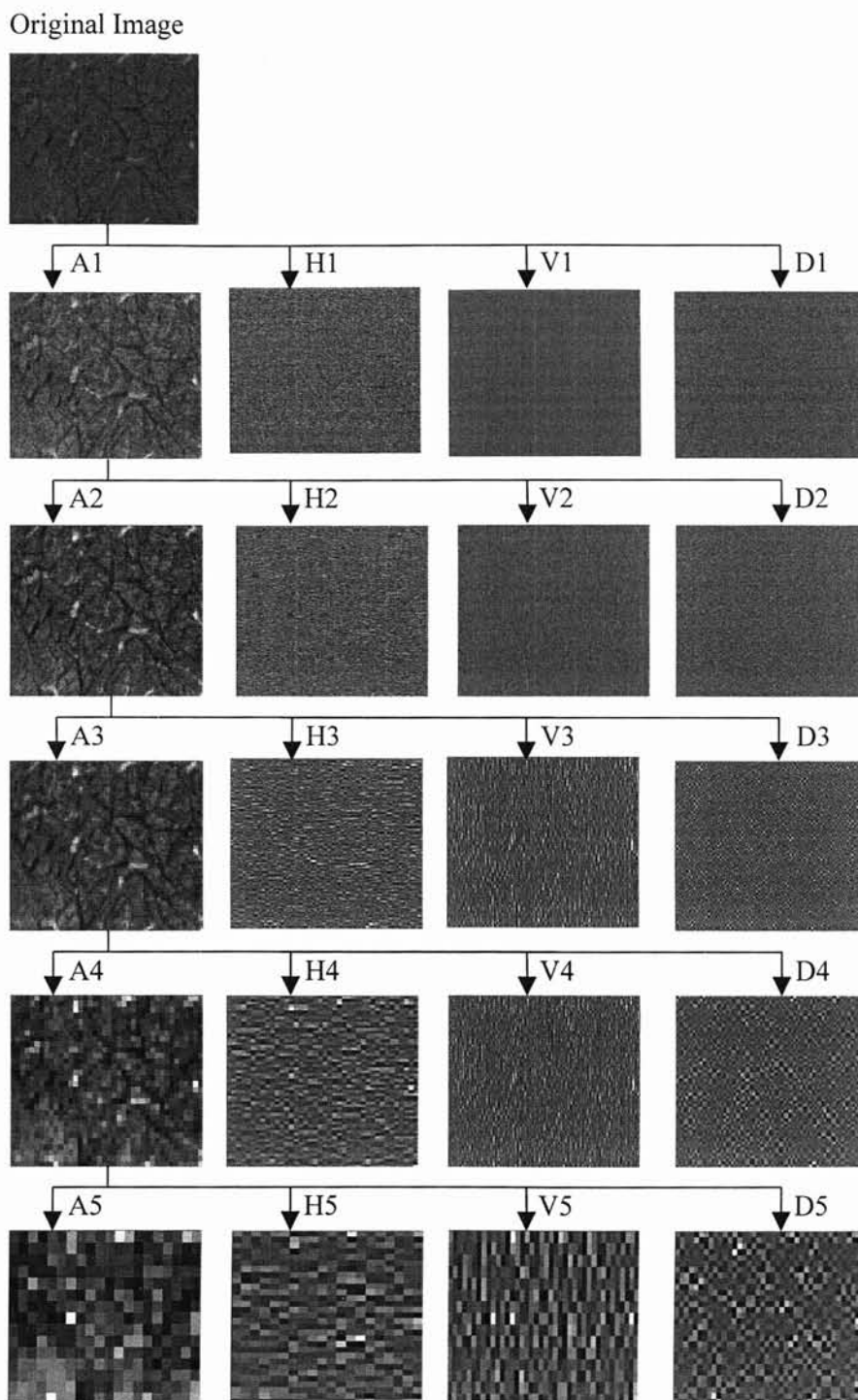
Figure 9. Five-level wavelet decomposition using Daubechies wavelets. A- approximation details; H- horizontal details; V- vertical details; D- diagonal details, from levels 1 to 5.

APPENDIX C- IMAGE ANALYSIS AND NEURAL NETWORK PROGRAMS

1. Function program to convert RGB color space to CIE L*a*b* (Jeyamkondan et al., 2001)

```
function [L, a, b]=rgb2Lab(rgb)

[h,w,b] = size(rgb);
rgbv = reshape (rgb, [h*w, b]);

[X, Y, Z] = rgb2xyz (rgbv);
Xr = X/95.04;
Yr = Y/100.0;
Zr = Z/108.89;

gy = Yr>0.008856;
fgY=gy.*(Yr.^(1/3));
Lg=(116*fgY-16).*gy;

ly = Yr<=0.008856;
Ll=903.3*Yr.*ly;
flY=(7.787*Yr+16/116).*ly;

L = Lg +Ll;
fY = fgY +flY;

gx = Xr>0.008856;
fgX=gx.*(Xr.^(1/3));

lx =Xr<=0.008856;
flX=(7.787*Xr+16/116).*lx;
fX = fgX+flX;

gz = Zr>0.008856;
fgZ=gz.*(Zr.^(1/3));
lz = Zr<=0.008856;
flZ=(7.787*Zr+16/116).*lz;
fZ = flZ+fgZ;

  a=500*(fX-fY);
  b=200*(fY-fZ);
  L = reshape (L, [h w]);
  a = reshape (a, [h w]);
  b = reshape (b, [h w]);
```

%Function to convert RGB color space to XYZ
function [x, y, z]=rgb2xyz(rgb)

```
r=double(rgb(:,1));
g=double(rgb(:,2));
b=double(rgb(:,3));

x= 0.4124*r+0.3576*g+0.1805*b;
y = 0.2126*r+0.7152*g+0.0722*b;
z = 0.0193*r+0.1192*g+0.9505*b;
```

2. Program for extracting WT-based textural features from wavelet decomposition images

```
%Creating a file for writing data
feat=fopen ('WT-Rspace.txt','w');
pref='OBIC';
path=[pwd '\'];
tic;
for filenum=1:186
file=strcat(pref,num2str(filenum),'.tif');
I = (imread([path file],'tif'));
```

% R color band of the RGB color space
```
x1=I(:,:,1);
```

% G color band of the RGB color space
```
x2=I(:,:,2);
```

% B color band of the RGB color space
```
x3=I(:,:,3);
```

% CIE L*a*b* color space calculation by calling the function program
```
[L, a, b] = rgb2Lab (I);
```

% Wavelet decomposition using Haar wavelet in R,G and B color bands, each band calculated separately
```
[C,S]=wavedec2(x1,5,'haar');
[C,S]=wavedec2(x2,5,'haar');
[C,S]=wavedec2(x3,5,'haar');
```

%Wavelet decomposition using Haar wavelet in L*,a* and b* color bands, each band calculated separately
```
[C,S]=wavedec2(L,5,'haar');
[C,S]=wavedec2(a,5,'haar');
[C,S]=wavedec2(b,5,'haar');
```

%Wavelet decomposition using Daubechies wavelet in R,G and B color bands, each band calculated separately

```
[C,S]=wavedec2(x1,5,'db2');
[C,S]=wavedec2(x2,5,'db2');
[C,S]=wavedec2(x3,5,'db2');
```

%Wavelet decomposition using Daubechies wavelet in L*,a* and b* color bands, each band calculated separately

```
[C,S]=wavedec2(L,5,'db2');
[C,S]=wavedec2(a,5,'db2');
[C,S]=wavedec2(b,5,'db2');
```

%Wavelet decomposition for contrast stretched images in R,G,and B color bands
//Contrast stretching operation

```
j=imadjust(x1, stretchlim(x1),[]);
j=imadjust(x2, stretchlim(x2),[]);
j=imadjust(x3, stretchlim(x3),[]);

j=double(j);
[C,S]=wavedec2(j,5,'haar');
[C,S]=wavedec2(j,5,'db2');
```

% Extracting wavelet coefficients from all levels

```
cA2 = appcoef2(C,S,'haar',5);
[cH5,cV5,cD5] = detcoef2('all',C,S,5);
[cH4,cV4,cD4] = detcoef2('all',C,S,4);
[cH3,cV3,cD3] = detcoef2('all',C,S,3);
[cH2,cV2,cD2] = detcoef2('all',C,S,2);
[cH1,cV1,cD1] = detcoef2('all',C,S,1);
```

%Reconstructing approximation coefficients from 1 to 5

```
A5 = wrcoef2('a',C,S,'haar',5);
A4 = wrcoef2('a',C,S,'haar',4);
A3 = wrcoef2('a',C,S,'haar',3);
A2 = wrcoef2('a',C,S,'haar',2);
A1 = wrcoef2('a',C,S,'haar',1);
```

% Reconstructing horizontal coefficients from 1 to 5

```
H5 = wrcoef2('h',C,S,'haar',5);
H4 = wrcoef2('h',C,S,'haar',4);
H3 = wrcoef2('h',C,S,'haar',3);
H2 = wrcoef2('h',C,S,'haar',2);
H1 = wrcoef2('h',C,S,'haar',1);
```

```
EA4= (1/X)*(sum(A4.^2));
EA3= (1/X)*(sum(A3.^2));
EA2= (1/X)*(sum(A2.^2));
EA1= (1/X)*(sum(A1.^2));

EH5= (1/X)*(sum(H5.^2));
EH4= (1/X)*(sum(H4.^2));
EH3= (1/X)*(sum(H3.^2));
EH2= (1/X)*(sum(H2.^2));
EH1= (1/X)*(sum(H1.^2));

EV5= (1/X)*(sum(V5.^2));
EV4= (1/X)*(sum(V4.^2));
EV3= (1/X)*(sum(V3.^2));
EV2= (1/X)*(sum(V2.^2));
EV1= (1/X)*(sum(V1.^2));

ED5= (1/X)*(sum(D5.^2));
ED4= (1/X)*(sum(D4.^2));
ED3= (1/X)*(sum(D3.^2));
ED2= (1/X)*(sum(D2.^2));
ED1= (1/X)*(sum(D1.^2));

EL5= (1/X)*(sum(L5.^2));
EL4= (1/X)*(sum(L4.^2));
EL3= (1/X)*(sum(L3.^2));
EL2= (1/X)*(sum(L2.^2));
EL1= (1/X)*(sum(L1.^2));

%Wedge calculation at each level using Sobel operator
rL5 = reshape(L5, [480 640]);
rL4 = reshape(L4, [480 640]);
rL3 = reshape(L3, [480 640]);
rL2 = reshape(L2, [480 640]);
rL1 = reshape(L1, [480 640]);

[BWLR5,thLR5] = EDGE(rL5,'sobel');
WED5 = sum(sum(BWLR5));
[BWLR4,thLR4] = EDGE(rL4,'sobel');
WED4 = sum(sum(BWLR4));
[BWLR3,thLR3] = EDGE(rL3,'sobel');
WED3 = sum(sum(BWLR3));
[BWLR2,thLR2] = EDGE(rL2,'sobel');
WED2 = sum(sum(BWLR2));
[BWLR1,thLR1] = EDGE(rL1,'sobel');
WED1 = sum(sum(BWLR1));
```

```
%Calculation of variance
VarA5=var(A5);
VarA4=var(A4);
VarA3=var(A3);
VarA2=var(A2);
VarA1=var(A1);

VarH5=var(H5);
VarH4=var(H4);
VarH3=var(H3);
VarH2=var(H2);
VarH1=var(H1);

VarV5=var(V5);
VarV4=var(V4);
VarV3=var(V3);
VarV2=var(V2);
VarV1=var(V1);

VarD5=var(D5);
VarD4=var(D4);
VarD3=var(D3);
VarD2=var(D2);
VarD1=var(D1);

%Calculation of skewness
SKA5=skewness(A5);
SKA4=skewness(A4);
SKA3=skewness(A3);
SKA2=skewness(A2);
SKA1=skewness(A1);

SKH5=skewness(H5);
SKH4=skewness(H4);
SKH3=skewness(H3);
SKH2=skewness(H2);
SKH1=skewness(H1);

SKV5=skewness(V5);
SKV4=skewness(V4);
SKV3=skewness(V3);
SKV2=skewness(V2);
SKV1=skewness(V1);

SKD5=skewness(D5);
```

```
SKD4=skewness(D4);
SKD3=skewness(D3);
SKD2=skewness(D2);
SKD1=skewness(D1);

%Calculation of kurtosis
KA5=kurtosis(A5);
KA4=kurtosis(A4);
KA3=kurtosis(A3);
KA2=kurtosis(A2);
KA1=kurtosis(A1);

KH5=kurtosis(H5);
KH4=kurtosis(H4);
KH3=kurtosis(H3);
KH2=kurtosis(H2);
KH1=kurtosis(H1);

KV5=kurtosis(V5);
KV4=kurtosis(V4);
KV3=kurtosis(V3);
KV2=kurtosis(V2);
KV1=kurtosis(V1);

KD5=kurtosis(D5);
KD4=kurtosis(D4);
KD3=kurtosis(D3);
KD2=kurtosis(D2);
KD1=kurtosis(D1);
```

% Spacing and tabs for writing data on the text file created by "fopen"
```
fprintf(feat,'%d\t%9.2f\t%9.2f\t%9.2f\t%9.2f\t%9.2f\t%9.2f\t%9.2f\t%9.2f\t%9.2f\t%
9.2f\t%9.2f\t%9.2f\t%9.2f\t%9.2f\t%9.2f\t%9.2f\t%9.2f\t%9.2f\t%9.2f\t%9.2f\t%9.2f
\t%9.2f\t%9.2f\t%9.2f\t%9.2f\t%9.2f\t%9.2f\t%9.2f\t%9.2f\t%9.2f\t%9.2f\t%
9.2f\t%9.2f\t%9.2f\t%9.2f\t%9.2f\t%9.2f\t%9.2f\t%9.2f\t%9.2f\t%9.2f\t%9.2f
\t%9.2f\t%9.2f\t%9.2f\t%9.2f\t%9.2f\t%9.2f\t%9.2f\t%9.2f\t%9.2f\t%9.2f\t%
9.2f\t%9.2f\t%9.2f\t%9.2f\t%9.2f\t%9.2f\t%9.2f\t%9.2f\t%9.2f\t%9.2f\t%9.2f
\t%9.2f\t%9.2f\t%9.2f\t%9.2f\t%9.2f\t%9.2f\t%9.2f\t%9.2f\n',filenum,EA5,EA4,EA3
,EA2,EA1,EH5,EH4,EH3,EH2,EH1,EV5,EV4,EV3,EV2,EV1,ED5,ED4,ED3,ED2,E
D1,EL5,EL4,EL3,EL2,EL1,WED5,WED4,WED3,WED2,WED1,VarA5,VarA4,Var
A3,VarA2,VarA1,VarH5,VarH4,VarH3,VarH2,VarH1,VarV5,VarV4,VarV3,VarV2,
VarV1,VarD5,VarD4,VarD3,VarD2,VarD1,SKA5,SKA4,SKA3,SKA2,SKA1,SKH5,
SKH4,SKH3,SKH2,SKH1,SKD5,SKD4,SKD3,SKD2,SKD1,SKV5,SKV4,SKV3,SK
V2,SKV1,KA5,KA4,KA3,KA2,KA1,KH5,KH4,KH3,KH2,KH1,KV5,KV4,KV3,KV
2,KV1,KD5,KD4,KD3,KD2,KD1);
```

```
filenum
end
fclose('all')
toc;
```

3. Function program for calculating GLDH-based features (Jeyamkondan et al., 2001)

```
function texture = gldh (Image, teta)

I = double (Image);

[h, w] = size (I);
Irv = reshape (I, h*w, 1);

len = length (Irv);

switch (teta)
```

%Calculating textural features at angle of 0° and distance of 1 pixel
```
case 0,

srv (1: len-480) = Irv (1: len-480) + Irv (481 : len);
srv (len-479: len) = Irv (len-479: len);

drv (1: len-480) = Irv (1: len-480) - Irv (481 : len);
drv (len-479: len) = Irv (len-479: len);
```

%Calculating textural features at angle of 45° and distance of 1 pixel
```
case 45,

srv (1: len - 481) = Irv (1: len - 481) + Irv (482 : len);
srv (len - 480: len) = Irv (len - 480: len);

drv (1: len - 481) = Irv (1: len - 481) - Irv (482 : len);
drv (len - 480: len) = Irv (len - 480: len);
```

%Calculating textural features at angle of 90° and distance of 1 pixel
```
case 90,

srv (1: len-1) = Irv (1:len-1) + Irv (2:len);
srv (len) = Irv(len);

drv (1: len-1) = Irv (1:len-1) - Irv (2:len);
```

80

```
drv (len) = Irv(len);
```

%Calculating textural features at angle of 135° and distance of 1 pixel
```
case 135,

srv(1) = Irv (1);
srv (2: len- 480) = Irv (2: len-480) + Irv (481 : len-1);
srv (len-479: len) = Irv (len-479: len);

drv(1) = Irv (1);
drv (2: len- 480) = Irv (2: len-480) - Irv (481 : len-1);
drv (len-479: len) = Irv (len-479: len);
end

sbin = 0:510;
hsrv = hist (srv, sbin);

dbin = -255:255;
hdrv = hist (drv , dbin);
psrv = hsrv/len;
pdrv = hdrv/len;
Gmean = mean(Irv);
sbin = sbin+1;
a1= sum(psrv.*(sbin-2*Gmean).^2);
b1 =  sum(pdrv.*(dbin.^2));
```

%Calculating correlation
```
corr = 0.5* (a1-b1);
texture(4) = corr;
```

%Calculating contrast
```
contrast = b1;
texture(5) = contrast;
```

%Calculating entropy
```
entropy = - sum (psrv.*log10(psrv+1)) - sum (pdrv.* log10(pdrv+1));
texture(6) = entropy*100;
```

%Calculating homogeneity
```
homogeneity = sum ((1./1+dbin.^2).*pdrv);
texture(7) = homogeneity;
```

%Calculating cluster shade
```
clshade = sum (((sbin - 2*Gmean).^3).*psrv);
texture(8) = clshade/1000;
```

%Calculating cluster prominence
clprom = sum (((sbin - 2*Gmean).^4).*psrv);
texture(9) = clprom/1000000;

4. Program for extracting GLDH-based features from wavelet decomposition images (Jeyamkondan et al., 2001)

%Creating a file for writing data
wavegdh= fopen('GLDH-Rspace.txt','w');
pref='OBIC';
path=[pwd '\'];
tic;
for filenum=1:186
file=strcat(pref,num2str(filenum),'.tif');
I = (imread([path file],'tif'));

%R color band of the RGB color space
x1=I(:,:,1);

%G color band of the RGB color space
x2=I(:,:,2);

%B color band of the RGB color space
x3=I(:,:,3);

%CIE L*a*b* color space calculation by calling the function program
[L, a, b] = rgb2Lab (I);

%Wavelet decomposition using Haar wavelet in R, G, and B color bands, each band calculated separately
[C,S]=wavedec2(x1,5,'haar');
[C,S]=wavedec2(x2,5,'haar');
[C,S]=wavedec2(x3,5,'haar');

%Wavelet decomposition using Haar wavelet in R, G, and B color bands, each band calculated separately
[C,S]=wavedec2(L,5,'haar');
[C,S]=wavedec2(a,5,'haar');
[C,S]=wavedec2(b,5,'haar');

%Wavelet decomposition using Daubechies wavelet in R, G, and B color bands, each band calculated separately
[C,S]=wavedec2(x1,5,'db2');

82

```
[C,S]=wavedec2(x2,5,'db2');
[C,S]=wavedec2(x3,5,'db2');
```

%Wavelet decomposition using Daubechies wavelet in R, G, and B color bands, each band calculated separately
```
[C,S]=wavedec2(L,5,'db2');
[C,S]=wavedec2(a,5,'db2');
[C,S]=wavedec2(b,5,'db2');
```

%Wavelet decomposition for contrast stretched images in R,G,and B color bands
//Contrast stretching operation
```
j=imadjust(x1, stretchlim(x1),[]);
j=imadjust(x2, stretchlim(x2),[]);
j=imadjust(x3, stretchlim(x3),[]);

j=double(j);
[C,S]=wavedec2(j,5,'haar');
[C,S]=wavedec2(j,5,'db2');
```

% Extracting wavelet coefficients from all levels
```
cA2 = appcoef2(C,S,'db2',5);
[cH5,cV5,cD5] = detcoef2('all',C,S,5);
[cH4,cV4,cD4] = detcoef2('all',C,S,4);
[cH3,cV3,cD3] = detcoef2('all',C,S,3);
[cH2,cV2,cD2] = detcoef2('all',C,S,2);
[cH1,cV1,cD1] = detcoef2('all',C,S,1);
```

%Reconstructing approximation coefficients from 1 to 5
```
A5 = wrcoef2('a',C,S,'db2',5);
A4 = wrcoef2('a',C,S,'db2',4);
A3 = wrcoef2('a',C,S,'db2',3);
A2 = wrcoef2('a',C,S,'db2',2);
A1 = wrcoef2('a',C,S,'db2',1);
```

% Reconstructing horizontal coefficients from 1 to 5
```
H5 = wrcoef2('h',C,S,'db2',5);
H4 = wrcoef2('h',C,S,'db2',4);
H3 = wrcoef2('h',C,S,'db2',3);
H2 = wrcoef2('h',C,S,'db2',2);
H1 = wrcoef2('h',C,S,'db2',1);
```

%Reconstructing diagonal coefficients from 1 to 5
```
D5 = wrcoef2('d',C,S,'db2',5);
D4 = wrcoef2('d',C,S,'db2',4);
D3 = wrcoef2('d',C,S,'db2',3);
```

```
D2 = wrcoef2('d',C,S,'db2',2);
D1 = wrcoef2('d',C,S,'db2',1);

%Reconstructing vertical coefficients from 1 to 5
V5 = wrcoef2('v',C,S,'db2',5);
V4 = wrcoef2('v',C,S,'db2',4);
V3 = wrcoef2('v',C,S,'db2',3);
V2 = wrcoef2('v',C,S,'db2',2);
V1 = wrcoef2('v',C,S,'db2',1);

% Reshaping the approximation levels from 1 to 5
A5 = reshape (A5, [prod(size(A2)) 1]);
A4 = reshape (A4, [prod(size(A2)) 1]);
A3 = reshape (A3, [prod(size(A2)) 1]);
A2 = reshape (A2, [prod(size(A2)) 1]);
A1 = reshape (A1, [prod(size(A2)) 1]);

% Reshaping the horizontal levels from 1 to 5
H5 = reshape (H5, [prod(size(H2)) 1]);
H4 = reshape (H4, [prod(size(H2)) 1]);
H3 = reshape (H3, [prod(size(H2)) 1]);
H2 = reshape (H2, [prod(size(H2)) 1]);
H1 = reshape (H1, [prod(size(H1)) 1]);

% Reshaping the diagonal levels from 1 to 5
D5 = reshape (D5, [prod(size(D2)) 1]);
D4 = reshape (D4, [prod(size(D2)) 1]);
D3 = reshape (D3, [prod(size(D2)) 1]);
D2 = reshape (D2, [prod(size(D2)) 1]);
D1 = reshape (D1, [prod(size(D1)) 1]);

% Reshaping the vertical levels from 1 to 5
V5 = reshape (V5, [prod(size(V2)) 1]);
V4 = reshape (V4, [prod(size(V2)) 1]);
V3 = reshape (V3, [prod(size(V2)) 1]);
V2 = reshape (V2, [prod(size(V2)) 1]);
V1 = reshape (V1, [prod(size(V1)) 1]);


%Calculating GLDH-based features for the approximation level, for 0°
texA5 = gdlh(A5,0);
texA4 = gldh(A4,0);
texA3 = gldh(A3,0);
texA2 = gldh(A2,0);
texA1 = gldh(A1,0);
```

%Calculating GLDH-based features for the horizontal level, for 0°
texH5 = gldh(H5,0);
texH4 = gldh(H4,0);
texH3 = gldh(H3,0);
texH2 = gldh(H2,0);
texH1 = gldh(H1,0);

%Calculating GLDH-based features for the vertical level, for 0°
texV5 = gldh(V5,0);
texV4 = gldh(V4,0);
texV3 = gldh(V3,0);
texV2 = gldh(V2,0);
texV1 = gldh(V1,0);

%Calculating GLDH-based features for the diagonal level, for 0°
texD5 = gldh(D5,0);
texD4 = gldh(D4,0);
texD3 = gldh(D3,0);
texD2 = gldh(D2,0);
texD1 = gldh(D1,0);

% Spacing and tabs for writing data on the text file created by "fopen"
fprintf(wavegdh,'%d\t%9.2f\t%9.2f\t%9.2f\t%9.2f\t%9.2f\t%9.2f\t%9.2f\t%9.2f\t%9.
2f\t%9.2f\t%9.2f\t%9.2f\t%9.2f\t%9.2f\t%9.2f\t%9.2f\t%9.2f\t%9.2f\t%9.2f\t%9.2f\t
%9.2f\t%9.2f\t%9.2f\t%9.2f\t%9.2f\t%9.2f\t%9.2f\t%9.2f\t%9.2f\t%9.2f\t%9.2f\t%9.
2f\t%9.2f\t%9.2f\t%9.2f\t%9.2f\t%9.2f\t%9.2f\t%9.2f\t%9.2f\t%9.2f\t%9.2f\t%9.2f\t
%9.2f\t%9.2f\t%9.2f\t%9.2f\t%9.2f\t%9.2f\t%9.2f\t%9.2f\t%9.2f\t%9.2f\t%9.2f\t%9.
2f\t%9.2f\t%9.2f\t%9.2f\t%9.2f\t%9.2f\t%9.2f\t%9.2f\t%9.2f\t%9.2f\t%9.2f\t%9.2f\t
%9.2f\t%9.2f\t%9.2f\t%9.2f\t%9.2f\t%9.2f\t%9.2f\t%9.2f\t%9.2f\t%9.2f\t%9.2f\t%9.
2f\t%9.2f\t%9.2f\t%9.2f\t%9.2f\t%9.2f\t%9.2f\t%9.2f\t%9.2f\t%9.2f\t%9.2f\t%9.2f\t
%9.2f\t%9.2f\t%9.2f\t%9.2f\t%9.2f\t%9.2f\t%9.2f\t%9.2f\t%9.2f\t%9.2f\t%9.2f\t%9.
2f\t%9.2f\t%9.2f\t%9.2f\t%9.2f\t%9.2f\t%9.2f\t%9.2f\t%9.2f\t%9.2f\t%9.2f\t%9.2f\t
%9.2f\t%9.2f\t%9.2f\t%9.2f\t%9.2f\t%9.2f\t%9.2f\t%9.2f\n',filenum,texA5(1),
texA5(2), texA5(3), texA5(4), texA5(5), texA5(6), texA4(1), texA4(2), texA4(3),
texA4(4), texA4(5), texA4(6), texA3(1), texA3(2), texA3(3), texA3(4), texA3(5),
texA3(6), texA2(1), texA2(2), texA2(3), texA2(4), texA2(5), texA2(6), texA1(1),
texA1(2), texA1(3), texA1(4), texA1(5), texA1(6), texH5(1), texH5(2), texH5(3),
texH5(4), texH5(5), texH5(6), texH4(1), texH4(2), texH4(3), texH4(4), texH4(5),
texH4(6), texH3(1), texH3(2), texH3(3), texH3(4), texH3(5), texH3(6), texH2(1),
texH2(2), texH2(3), texH2(4), texH2(5), texH2(6), texH1(1), texH1(2), texH1(3),
texH1(4), texH1(5), texH1(6), texV5(1), texV5(2), texV5(3), texV5(4), texV5(5),
texV5(6), texV4(1), texV4(2), texV4(3), texV4(4), texV4(5), texV4(6), texV3(1),
texV3(2), texV3(3), texV3(4), texV3(5), texV3(6), texV2(1), texV2(2), texV2(3),
texV2(4), texV2(5), texV2(6), texV1(1), texV1(2), texV1(3), texV1(4), texV1(5),
texV1(6), texD5(1), texD5(2), texD5(3), texD5(4), texD5(5), texD5(6), texD4(1),

texD4(2), texD4(3), texD4(4), texD4(5), texD4(6), texD3(1), texD3(2), texD3(3), texD3(4), texD3(5), texD3(6), texD2(1), texD2(2), texD2(3), texD2(4), texA2(5), texA2(6), texV1(1), texV1(2), texV1(3), texV1(4), texV1(5), texV1(6));

```
filenum
end
fclose('all')
toc;
```

5. Program for predicting WBS scores using BPNN with Bayesian regularization

p=[*WT- or GLDH-based textural features*];

tc=[*WBS scores obtained from Department of Animal Science Meat Laboratory*]';

t = tc(1,:);

% Normalizing the data
[pn,meanp,stdp,tn,meant,stdt] = prestd(p,t);

% Principal component analysis
[ptrans,transMat] = prepca(pn,0.01);
[R,Q] = size(ptrans);

%Test Set
iitst = 2:4:Q;

%Training Set
iitr = [1:4:Q 3:4:Q 4:4:Q];
test.P = ptrans(:,iitst); test.T = tn(:,iitst);
ptr = ptrans(:,iitr); ttr = tn(:,iitr);

%Creating a feed-forward BPNN with bayesian regularization training. One output neuron, with linear transfer function and 10 and 20 neurons in the hidden layer, with logsigmoid and tansigmoid transfer functions

net = newff(minmax(ptr),[10 20 1],{'logsig' 'tansig' 'purelin'},'trainbr');
net.trainParam.show = 10;
net.trainParam.epochs = 50;

%Training the network
[net,tr]=train(net,ptr,ttr);
antr = sim(net,ptrans(:,iitr));

% Un-normalizing the output which had been normalized by PRESTD.
atr = poststd(antr,meant,stdt);

%Post-processing the network training set by performing a linear regression between one element of the network response and the corresponding target
[m,b,r] = postreg(atr,t(:,iitr));

antst = sim(net,ptrans(:,iitst));
atst = poststd(antst,meant,stdt);

[m,b,r] = postreg(atst,t(:,iitst));

VITA ⱥ

Anand Lakshmikanth

Candidate for the Degree of

Master of Science

Thesis: PREDICTING TENDERNESS OF BEEF USING MACHINE VISION

Major Field: Biosystems Engineering

Biographical:

Personal: Born in Karur, Tamilnadu, India on May 10th 1974, the son of P.R. Lakshmikanthan and S. Visalakshi.

Education: Graduated from D.T.E.A. Senior Secondary School, New Delhi, India in May 1992; received Bachelor of Engineering Degree in Agriculture from College of Agricultural Engineering, Tamil Nadu Agricultural University (TNAU), Kumulur, Tamilnadu, India in June 1998. Completed the requirements for Master of Science degree with a major in Biosystems Engineering at Oklahoma State University in December 2002.

Experience: Employed by Oklahoma State University as Graduate Research Assistant in the Department of Biosystems and Agricultural Engineering from July 2000 to present.

Professional Memberships: American Society of Agricultural Engineers.